Genotype tunes pancreatic ductal adenocarcinoma tissue tension to induce matricellular fibrosis and tumor progression

Genotype tunes PDAC tension to drive matricellular-enriched fibrosis and tumor aggression

Hanane Laklai[1], Yekaterina A. Miroshnikova[1], Michael W. Pickup[1], Eric Collisson[2], Grace E. Kim[3], Alex S. Barrett[4], Ryan C. Hill[4], Johnathon N. Lakins[1], David D. Schlaepfer[5], Janna K. Mouw[1], Valerie S. LeBleu[6], Sergey V. Novitskiy[7], Julie S. Johansen[8], Valeria Poli[9], Kirk Hansen[4], Raghu Kalluri[6], Harold L. Moses[7] and Valerie M. Weaver[1, 10-13]

[1]Center for Bioengineering and Tissue Regeneration, Department of Surgery, University of California, San Francisco, San Francisco, CA, 94143, USA
[2]Department of Medicine, University of California, San Francisco, San Francisco, CA, 94143
[3]Department of Pathology, University of California, San Francisco, San Francisco, CA, 94143, USA
[4]Department of Biochemistry and Molecular Genetics, University of Colorado, Denver, Aurora, CO 80045, USA
[5]Departments of Reproductive Medicine, University of California, San Diego Moores Cancer Center, La Jolla, CA, 92093, USA
[6]Department of Integrative Biology and Pharmacology, University of Texas Health Science Center at Houston–Medical School, Houston, TX, 77225, USA
[7]Department of Cancer Biology, Vanderbilt University School of Medicine and Vanderbilt-Ingram Cancer Center, Nashville, TN, 37232, USA
[8]Department of Oncology, Herlev Hospital, Copenhagen University Hospital, Copenhagen, Denmark
[9]Molecular Biotechnology Center and Department of Genetics, Biology and Biochemistry, University of Turin, Turin, 10126, Italy
[10]Department of Anatomy and Department of Bioengineering and Therapeutic Sciences, University of California, San Francisco, San Francisco, CA, 94143, USA
[11]Eli and Edythe Broad Center of Regeneration Medicine and Stem Cell Research, University of California, San Francisco, San Francisco, CA, 94143, USA
[12]UCSF Helen Diller Comprehensive Cancer Center, University of California, San Francisco, San Francisco, CA, 94143,USA

[13]Correspondence to:
Valerie M. Weaver
Center for Bioengineering and Tissue Regeneration
Department of Surgery
University of California, San Francisco
513 Parnassus Avenue, HSE-565
San Francisco, CA 94143
Email: Valerie.Weaver@ucsf.edu
Telephone: (415) 476-3826

Abstract

The fibrotic phenotype of pancreatic ductal carcinoma contributes to patient mortality. Nevertheless, anti-stromal therapies have had mixed results, suggesting there are multifaceted, anti and pro-tumorigenic roles for fibrosis. We found that the genotype of pancreatic ductal carcinomas tunes the tension of the malignant epithelium to mechanically prime the stroma and promote tumor progression through epithelial pSTAT3 and YAP. Kras pancreatic tumors in mice lacking epithelial TGFβ signaling developed a highly stiff, matricellular-enriched fibrosis and exhibited increased epithelial myosin activity with elevated cytokine, Jak, Rock, Fak and Yap signaling, and Stat3-dependent inflammation. Increasing pancreatic epithelial mechanosignaling accelerated Kras-dependent transformation that was accompanied by stromal stiffening and a matricellular-enriched fibrosis with high epithelial Yap and pStat3 activity. Elevating pStat3 increased tissue tension and matricellular-enriched fibrosis and activated Yap to accelerate Kras-dependent pancreatic transformation. By contrast, epithelial Stat3 ablation attenuated pancreatic malignancy and reduced the matricellular-enriched fibrosis, stromal stiffening, epithelial contractility and Yap activation induced by Kras/TGFβ knockout. Tissue arrays revealed that the least differentiated human pancreatic tumors from patients with the shortest survival had matricellular-enriched fibrosis and a highly contractile, mesenchymal-like epithelium that lacked pSMAD and had elevated pSTAT3, YAP and SOX2. Our data underscore the importance of tumor genotype in tuning stromal-epithelial interactions and illustrate how tissue tension can force malignancy, drive tumor aggression and compromise patient survival.

Introduction

Pancreatic ductal adenocarcinomas (PDACs) are profoundly fibrotic and PDAC patients have a high mortality rate[1]. PDAC fibrosis induces interstitial fluid pressure to disrupt blood vessel integrity and induce hypoxia that compromise drug delivery and promote disease aggression and therapy resistance[2–5]. Consequently, considerable resources have been expended to develop strategies to reduce PDAC fibrosis[6]. To this end, inhibition of stromal sonic hedgehog (SHH) signaling in a mouse model of PDAC significantly reduced fibrosis and increased intratumoral vascular density to increase drug update that, at least transiently, stabilized the disease[7]. Similarly, reducing mouse pancreatic tumor hyaluronan, using hyaluronidase, or treating xenografted human pancreatic tumors with an angiotensin inhibitor to reduce tissue tension, decreased interstitial fluid pressure and normalized the vasculature to facilitate chemotherapy response[8,9]. Yet, phase II clinical trials in PDAC patients treated with the SHH inhibitors IPI-926 or GDC-0449, or with a monoclonal antibody against the collagen cross-linking enzyme LOXL2, failed (NCT01472198)[10]. Experiments in mouse models of PDAC revealed that, while depletion of proliferating α-smooth muscle actin (αSMA) positive stromal cells reduced fibrosis, the vasculature remained abnormal and the tumor, while smaller, was hypoxic and less differentiated, with accelerated mortality[11]. Despite a frank reduction in fibrosis and enhancement of tissue vascularity, genetic ablation of SHH or treatment with a smoothened inhibitor induced mouse PDACs that were less differentiated and more, not less, aggressive[12]. These data imply that the stroma can both promote and restrain tumor progression, and suggest stromal dependency may be context dependent. Whether such complexity could be explained by distinct tumor genotype - stromal interactions or by the natural evolution of PDACs remains unclear.

Malignant transformation of an epithelial tissue is universally accompanied by extracellular matrix (ECM) deposition and remodeling[13,14]. Nevertheless, the extent and nature of the fibrosis and the responsiveness of the transformed epithelium to the desmoplastic ECM can vary widely across cancers, amongst tumor subtypes and even within one tumor[15–18]. Indeed, the fibrotic response in patients with aggressive, treatment-resistant, quasi-mesenchymal PDACs (QM-PDA) is less prominent and tumor cells isolated from QM-PDA patients are only marginally anchorage-dependent for their growth and survival[19,20]. By contrast, patients with classical PDACs have a better prognosis and classical PDACs are more differentiated, and tumor

cells isolated from these cancers retain Ras dependence and express higher levels of cell adhesion molecules[11,21]. Although the origins of the QM and classical histophenotypes have yet to be determined, PDAC development has been irrevocably linked to a handful of genetic modifications. Thus, pre-malignant pancreatic lesions (PanINs) frequently possess activating point mutations in the *Kras* proto-oncogene and PDAC progression correlates with either the genetic and/or epigenetic inactivation of the tumor suppressor genes *p16INK4a* (<90%), *p53* (<75%) and *SMAD4* (*DPC4*, <55%)[22]. Consistently, genetically-engineered mouse models (GEMMs) in which an activated Kras is expressed in the pancreatic ductal epithelium develop PanINS and when combined with deletion of a single allele of p53, p16INK4a, Smad4 or Tgfbr2 develop PDACs[23–26]. Of these genetic modifications, mice with combined Kras mutations and Tgfbr2 deletion are very aggressive and exhibit a mesenchymal-like phenotype following stromal ablation[11,23]. Moreover, the human mesenchymal-like PDAC phenotype most frequently associates with aberrant TGFβ signaling in the epithelium[27]. These findings imply that distinct genotypes may dictate unique stromal-epithelial phenotypes. Importantly, as mouse PDACs develop they also increase expression of mesenchymal-like features, as do patients with recurrent PDACs, and ablation of proliferating alpha smooth muscle actin (αSMA) positive cells in Kras/p53 mouse PDAC permits the expansion of mesenchymal-like, aggressive tumors[28–30]. These observations suggest that the epithelium likely evolves over time towards a less stromally-dependent phenotype and imply that this evolution may be linked to the engagement of pathways that promote a mesenchymal-like transition.

High grade PDACs express more Sex-determining region Y (SRY)-Box2 (SOX2), a transcription factor that drives an epithelial-to-mesenchymal transition (EMT), with elevated Sox2 levels in PDACs linked to poor PDAC patient prognosis[31,32]. Poorly differentiated, mesenchymal-like PDACs (QM-PDACs) also express higher levels and activity of the Hippo transcription factor Yes-associated protein 1 (YAP), and YAP directly induces SOX2 and an EMT[20,33–37]. These findings suggest QM-PDACs may arise through elevated YAP and SOX2 activity. YAP is exquisitely sensitive to mechanical stimuli such that cells interacting with a stiff ECM activate more ROCK to increase nuclear YAP and induce YAP-dependent gene expression[38,39]. Importantly, PDACs are mechanically-activated tumors composed of a progressively stiffened ECM and high interstitial pressure[2,8,11]. Thus, the elevated tissue mechanics mediated by the stiffened tissue stroma and high interstitial pressure could eventually

activate YAP to drive tumor aggression and induce an EMT. Yet, many oncogenes also induce tissue tension by increasing Rock-dependent contractility. Indeed, the majority of PDACs have activated Kras, and Kras activity, per se, increases ROCK to drive cell contractility which, in turn, induces ECM remodeling and stiffening to drive integrin-dependent mechanosignaling and malignant transformation[40,4142]. It is therefore also equally plausible that the genotype of the pancreatic tumor epithelium additionally elevates tissue tension to drive tumor progression. Here, we examined human pancreatic tumor tissue of differing grades and survival, and exploited a series of PDAC GEMMs to explore the relationship between tumor genotype, stromal-epithelial interactions and tissue tension in PDAC progression and aggression.

Results

Human PDAC aggression is characterized by low epithelial TGFβ signaling and high myosin activity

PDACs are fibrotic, and contain abundant fibrillar collagen[1].Yet, recent findings suggest collagen abundance may associate with better, not worse, patient prognosis and that high collagen content correlates with a more differentiated PDAC phenotype[43–45]. Nevertheless, high fibrillar collagen has repeatedly been implicated in PDAC aggression and treatment resistance[46]. To address this discrepancy, we constructed a gene list of major fibrillar collagens (Supplementary Table 1) and used this signature to interrogate a publically-available NCBI GEO agilent gene expression data set (GSE21501) consisting of 67 PDAC patients between the ages of 40 and 65. We could find no statistical differences in the combined expression levels of the major fibrillar collagens and patient survival. However, when we created a median centroid value representing an average high versus low Col1α2, Col2α1 and Col4α1 combined expression score for each patient and graphed each of the groups over time, a Cox-Mantel Log-rank analysis revealed that patients with high levels of these fibrillar collagens had a reduced overall survival, as illustrated by Kaplan-Meier survival curves (log rank $p \leq 0.04$; Fig. 1a). These data suggest elevated gene expression of specific fibrillar collagens can predict poorer patient outcome.

Collagens are subjected to a plethora of posttranslational modifications that can modify their organization and mechanical properties. Therefore, to more directly investigate the relationship between fibrillar collagens and PDAC tumor phenotype, we secured PDAC tissue

arrays from US Biomax representing a total of 68 patients between the ages of 23 and 78 with well (n=19), moderately (n=23) and poorly differentiated (n=26) tumors. A UCSF pathologist confirmed tumor grade using H&E stained sections. Thereafter, serial sections were stained for total collagen using Massons Trichrome and assessed for fibrillar collagen levels, organization and diameter using polarized imaging of Picrosirius Red (PR) stained tissue and second-harmonic generation (SHG). A superficial analysis of the H&E and trichrome stained images implied that the poorly differentiated PDACs contained reduced stroma and total collagen, consistent with the reduced level of alpha smooth muscle actin (αSMA) positive cells we also detected (Fig. 1b,b')[11,47]. Nevertheless, quantification of PR stained, polarized images revealed there was a modest, albeit non-significant, increase in total fibrillar collagen in the least differentiated tumors (Fig. 1 b, b'). Furthermore, quantitative analysis of SHG images revealed that the collagen fiber diameter was significantly thicker in the poorly differentiated PDACs, suggesting higher localized tissue tension. Indeed, additional analysis revealed there was a significant and progressive increase in levels of pMLC2, reflecting higher mechanosignaling in the epithelium of the moderately and poorly differentiated tumors (Fig. 1b, b'). Moreover, upon further examination, we established an inverse relationship between levels of nuclear pSmad and PDAC differentiation (Fig. 1b, b').

To further interrogate the relationship between fibrillar collagen phenotype, mechanosignaling and patient survival, we secured a set of tissues from a 57 patient PDAC cohort representing patients with a median short survival of less than 10 months (n=29) as compared to a median long-term survival of over 24 months (n=28) [48]. Consistent with prior findings, Massons Trichrome stained tissue and polarized imaging of PR stained sections indicated there was no consistent relationship between total and fibrillar collagen or αSMA positive stained cells in the tissues from patients with the short versus the longer survival (Fig. 1c, c'). However and importantly, we again found that fiber diameter was significantly thicker in those patients with the shortest survival, as revealed by SGH. We also noted that the PDAC tissues from patients with the shortest survival contained the highest amount of epithelial pMLC2, suggesting they had elevated mechanosignaling and tissue tension (Fig. 1c, c'). Moreover, once again, the epithelium in the PDAC tissue excised from the patients with the shortest survival also had low to negligible detectable pSmad (Fig. 1c, c'). These findings indicate collagen organization and tissue tension, and not collagen abundance, are more robust

indicators of PDAC aggression. The data also suggest reduced TGFβ signaling in the PDAC epithelium may alter stromal-epithelial interactions to drive tumor aggression.

Tumor genotype tunes epithelial tension to regulate the fibrotic phenotype

To explore the relationship between TGFβ signaling and tissue mechanics, the fibrotic phenotype and tumor aggression we exploited available PDAC GEMMs. We used a GEMM in which mutant Kras was conditionally expressed in the pancreatic epithelial cells ($Kras^{LSL\text{-}G12D/+}$; Ptf1α-Cre; KC)[49] either alone or in combination with mice heterozygous for mutant P53 ($Kras^{LSL\text{-}G12D/+}$;$TrP53^{R172H/+}$; Pdx1-Cre; KPC), lacking one allele of P53 ($Kras^{LSL\text{-}G12D/+}$;$TrP53^{flox/wt}$; Ptf1α; KP-Ptf1α-C) or those lacking one allele of the TGFβ receptor II ($Kras^{LSL\text{-}G12D/+}$;$Tgfbr2^{flox/wt}$; Ptf1a-Cre; KTC). As has been previously reported, by 20 weeks Kras mice had progressed to PanIN lesions, whereas both the KPC and KTC mice developed frank PDACs[23,24]. Coincident with tumor formation, the pancreatic tissue of both the KPC and KTC mice was highly fibrotic, as indicated by abundant quantities of total and fibrillar collagen (not shown). Mass spectroscopy proteomics analysis confirmed that many of the fibrillar collagens in the KTC and KPC mice were present at similar levels (Supplementary Table 2) and immunofluorescence staining revealed that both mouse GEMM PDACs had similar levels collagen III and numbers of αSMA and FAP positive cells throughout their stroma (Supplementary Fig. 2a). Gli-1, which regulates PDAC fibrosis, was also abundantly and uniformly expressed equally in the stroma in both PDAC models (Supplementary Fig. 2a). Nevertheless, and in agreement with our clinical findings, PR and SHG imaging revealed that the PDACs in the KTC mice had significantly thicker collagen bundles that were particularly evident in the region surrounding the tumor epithelium, which atomic force microscopy (AFM) indicated was significantly stiffer than the stroma surrounding the KPC tumor epithelium (Fig. 2a, a', a"). Upon further scrutiny, we noted that the altered fibrillar collagen phenotype and the elevated stromal stiffness in the KTC PDACs was accompanied by a significant increase in levels of matricellular proteins including tenascin C, fibronectin and collagen XIIA (Fig. 2a, b). The epithelium of the KTC PDACs also had higher mechanosignaling, as revealed by more activated β1 integrin and ^{p397}FAK, with greater nuclear levels of the mechano-activated transcription factor YAP (Fig. 2a). These findings indicate that loss of pancreatic epithelial TGFβ signaling induces a mechanically-activated, matricellular-enriched fibrotic phenotype.

Importantly and consistent with our clinical findings, we quantified more pMLC2 and pMyPT1 in the epithelium of the KTC PDACs, implicating loss of TGFβ signaling in the elevated tissue mechanics (Fig. 2a). Indeed, traction force microscopy (TFM), which quantifies the contractility phenotype of individual cells, revealed that freshly isolated pancreatic KTC tumor cells and cultured pancreatic Kras tumor cells lacking Tgfbr2 expression were significantly more contractile (Fig. 2c, c'). Further studies confirmed this observation and showed the KTC tumor cells were able to induce more ROCK-dependent collagen gel contraction than isolated cancer cells from KPC or KC mouse tumors (Fig. 2d, d' and supplementary Fig. 3a, a'). The KTC pancreatic tumor cells also drove more ROCK-dependent collagen gel remodeling and stiffening (Fig. 2a, a' and Supplementary Fig. 3a, a', b, b'), more ROCK-dependent fibrosis and tissue stiffening when injected into the pancreas of immune-compromised mice, and activated more Yap as indicated by higher nuclear levels and increased CTGF expression (Fig. 2e, e', e" and Supplementary Fig. 3c", c"'). Not only were the pancreatic tumor cells able to directly promote ROCK-dependent tissue fibrosis, but the phenotype was independent of proliferation with the non-fibrotic KPC pancreatic tumor cells forming larger, not smaller, tumors than those generated by the control and ROCK-knockdown KTC tumor cells (Supplementary Fig. 3c, c'). Thus, although pancreatic transformation is universally accompanied by a progressive fibrosis and stiffening of the ECM, the nature of the fibrotic response and the mechano-phenotype of the cancer can be modified by the genotype of the tumor. In particular, loss of TGFβ signaling in the epithelium can increase cancer cell contractility to "tune" the mechano-fibrotic phenotype of the malignant tissue.

Loss of TGFβ signaling activates a JAK/Stat3 contractility feed forward circuit to induce ECM remodeling and tissue stiffening

G protein coupled receptor (GPCR)-mediated JAK activation not only stimulates Stat3 but activates ROCK and induces actomyosin-mediated cell contractility[50] and GPCR activation can activate Yap[39]. Stat3 activity is frequently elevated in pancreatic tumors[51,52] and KTC tumors express elevated cytokines. We therefore tested whether the matricellular fibrosis and elevated mechano-phenotype observed in the KTC mice could be mediated through elevated pancreatic epithelial GPCR-JAK-ROCK-Stat3[53]. In keeping with this paradigm, we noted that pStat3 staining was, indeed, significantly higher in the pancreatic epithelium of the KTC mice (Fig. 3a,

a'), even in the eight week old PanINs where the amount of infiltrating immune cells is quite low (Supplementary Fig. 4a, a'). Indeed, while both the stroma and the PDACs in the KPC and KTC mice stained positively for pStat3, coincident with an abundant immune infiltrate[53], pStat3 was consistently higher in the KTC tumor pancreatic epithelium (Fig. 3a, a'). We also detected abundant pStat3 in non-stimulated, pancreatic epithelial cells isolated from KTC tumors, whereas no activity was detected in either the newly isolated KPC and KC tumor cells (Fig. 3b). Moreover, the ability of the KTC tumor cells to contract collagen gels and to induce collagen remodeling was blocked by treatment with the JAK inhibitor Ruxolitinib (Fig. 3c, c", c"' and Supplementary Fig. 4b). We also noted that the 48 hour conditioned media from KTC tumor cells activated pStat3 in cultured KC cells (Fig. 3d, d'), and stimulated KC cell contraction and collagen remodeling, suggesting KTC cells secrete cytokines capable of inducing GPCR-JAK-ROCK-dependent contractility (Fig. 3e, e', e" and Supplementary Fig. 4c). Importantly, a stiff ECM can enhance GPCR-dependent Stat3 activation, and we observed higher steady state epithelial pStat3 and quantified higher levels of secreted cytokines in the media of Kras pancreatic tumor cells plated on a stiff ECM (Fig. 3f, f', g and Supplementary Fig. 4d, d', e). These findings not only identify epithelial JAK-ROCK-Stat3 signaling circuit as a candidate KTC tumor cell-specific contractility mechanism that could drive ECM remodeling and pancreatic fibrosis, they also imply that once stiffened, the rigid ECM will potentiate the activity of this pathway and would promote tumor aggression by activating mechano-activated pathways including Yap[20].

Tumor cell tension induces JAK-Stat3 signaling and matricellular fibrosis to accelerate Kras PDAC

To directly test whether epithelial contractility, per se, could induce matricellular fibrosis and PDAC progression we crossed transgenic mice expressing Ptf1α-Cre with mice expressing a conditional V737N β1 integrin, which recapitulates tension-dependent integrin clustering and promotes focal adhesion signaling to induce ROCK-dependent cell contractility in the pancreatic epithelium(Supplementary Fig. 5a) [40,54,55]. Immunofluorescence staining for ^{p397}FAK confirmed elevated focal adhesion kinase activity in the pancreatic epithelium in the β1V737N mice, revealed higher epithelial contractility by increased pMLC2 and higher mechano-signaling by elevated nuclear Yap targets such as CTGF (Supplementary Fig. 5b, c). Increased ductal

collagen was indicated by intense PR staining around the epithelium (Supplementary Fig. 5b) while SHG revealed thicker, denser collagens (not shown), and AFM indentation quantified a stiffened ECM surrounding the ductal epithelium (Supplementary Fig. 4b). The presence of pStat3 positive pancreatic epithelial cells in the β1V737N mice, even in the absence of any activating oncogene or pre-existing inflammation, confirmed that epithelial tension can enhance p Stat3 (Supplementary Fig. 5b), a finding that we verified in a mouse cohort treated with a FAK inhibitor by the loss of pStat3 together with reduced ^{p397}FAK, pMLC2 and matricellular fibrosis (Supplementary Fig. 6a, a'). Consistently, pancreatic orthotopic tumors formed by KTC cells lacking FAK were less fibrotic, and the tumors were softer and lacked epithelial pStat3 (Fig. 4e, e', e" and Supplementary Fig. 7a, a', b).

To directly assess the relationship between epithelial mechanosignaling and PDAC development, we bred Ptf1α-Cre V737N β1 integrin mice with KC mice and monitored the animals for development of matricellular fibrosis, elevated tissue mechanics, pStat3 signaling and tumor formation (Fig. 4a). As early as 5 weeks of age, the pancreatic epithelium in the KC mice expressing the β1V737N transgene had high ^{p397}FAK and pMLC2 activity, and the amount and distribution of deposited collagen and ECM stiffening was highest around the ductal epithelium (Fig. 4b, 4b'), and markedly similar to what we documented in the developing KTC lesions (compare SHG in Fig. 2a to PR in Fig. 4b). Moreover, consistent with the matricellular fibrosis observed in the patient samples lacking pSmad and the KTC lesions, we also detected abundant tenascin and higher levels of epithelial pStat3 in the KC/β1V737N mice (Fig. 4b, b'). This was accompanied by a significant increase in infiltrating CD45 immune cells (Supplementary Fig. 7c) and CD68 macrophages (Fig. 4b, b'), which FACS analysis suggested were tumor promoting (Supplementary Fig. 7c). Indeed, cytokine array analysis demonstrated that the KC/β1V737N mouse pancreas expressed significantly higher levels of pro-inflammatory factors C5α and IL1 (Supplementary Fig. 7d, d'). Finally and importantly, histological analysis confirmed that KC/β1V737N mice developed chronic pancreatitis as early as 3 months of age (Fig. 4c). Alcian blue staining of 3 month old KC/V737N mouse pancreatic tissue revealed that they had progressed to advanced, high grade PanINs that were evenly distributed throughout the tissue and H&E showed that 38% of the animals developed frank PDAC by 5-8 months of age, with accompanying physiological trauma including loss of body weight (Fig. 4c, c', d). These results reveal that tumor cells with elevated mechano-signaling are more contractile and, by

virtue of their ability to stiffen the ECM, induce matricellular fibrosis, activate tension-regulated genes and stimulate an immune response, can promote pancreatic transformation.

Stat3 induces tissue fibrosis to accelerate Kras-induced PDAC

We next explored the relationship between activated Stat3, cell contractility and pancreatic matricellular-enriched fibrosis in PDAC. KC mice were crossed into mice expressing one allele of a constitutively active Stat3 (Stat3C, Fig. 5a)[56]. We first noted that Stat3C mice contained numerous cells within the pancreas that stained positively for activated Stat3 (Supplementary Fig. 9a, a') and that the level of pStat3 increased dramatically following expression of an activated Kras (Fig. 5b, b'). We also quantified higher numbers of CD45 immune cells and CD68 macrophages within the Stat3C pancreatic tissues (Supplementary Fig. 9a, a') and that these increased substantially with Kras activation, consistent with induction of a pro-inflammatory phenotype (Fig. 5b, b'). Indeed, the pancreatic tissues of the Stat3C/Kras mice showed marked pancreatitis that developed into frank PDAC, which compromised the survival of the mice (Fig. 5c). Consistent with a link between JAK/Stat3 activity and ROCK activity, immunofluorescence staining revealed that, while tumors were stiffer and pMLC2 was quite high in the KC/Stat3C mice, pMLC2 levels were already elevated in the pancreatic tissues of the Stat3C mice, even in the absence of Kras (Fig. 5b, b', d and Supplementary Fig. 9a, a'). Polarized light imaging of PR stained tissue revealed that the pancreas of the Stat3C mice already contained abundant mature type I collagen (Supplementary Fig. 9a, a'). Indeed, we were able to detect elevated ^{p397}FAK throughout the pancreas of the Stat3C mice (Supplementary Fig. 9a, a'). These findings not only demonstrate that there are links between pStat3 and tissue inflammation, but they also suggest that pStat3 induces ROCK-dependent ECM remodeling and stiffening to drive matricellular fibrosis and mechanosignaling in PDAC.

Stat3 enhances epithelial contractility to induce PDAC matricellular fibrosis and tumor aggression to compromise patient survival

To establish a causal relationship between pStat3, tissue mechanics and PDAC development, we crossed mice expressing Kras ($Kras^{LSL\text{-}G12D/+}$) with mice homozygous for loss of both of the TGF β receptor 2 alleles ($Tgfbr2^{flox/flox}$, which exhibit an accelerated matricellular fibrotic phenotype and PDAC development, Supplementary Fig. 8a, b) and Stat3 both in the pancreatic epithelium

(Stat3$^{flox/flox}$, Ptf1a-Cre) to create KTC KO/Stat3 KO mice (Fig. 5e)[23,57]. Immunostaining confirmed efficient deletion of Stat3 in the pancreatic epithelium (Fig. 5f, f') and showed that this was accompanied by reduced CD68 tissue infiltration, consistent with decreased inflammation (Fig. 5f, f'). Loss of epithelial pStat3 was also accompanied by a significant reduction in epithelial ^{p397}FAK, pMLC2 and nuclear Yap levels and activity as indicated by lower CTGF expression (Fig. 5f, f' and Supplementary Fig. 9b). Also, pancreatic tissues with deleted epithelial Stat3 presented with a striking reduction in matricellular-rich fibrosis and ECM stiffness, along with increased survival (Fig. 5f, f', g, h). Direct links between matricellular-rich fibrosis, mechanics and Stat3 were confirmed in a cohort of mice treated with the JAK inhibitor Ruxolitinib, which not only inhibited pStat3 activity but also reduced ^{p397}FAK, pMLC2, collagen fibrillogenesis and ECM stiffening (Supplementary Fig. 9c, c', d) as well as Yap activation (not shown). Moreover, in the absence of JAK-driven matricellular-rich fibrosis, mechanosignaling, Stat3-dependent inflammation and PDAC development were reduced (Supplementary Fig. 9c, c', e). Thus, tumor cell pStat3 not only stimulates inflammation, but increases epithelial cell tension and activates mechanosignaling to drive matricellular fibrosis and promote PDAC development and tumor aggression. Importantly and of clinical relevance, we detected elevated levels of tenascin and high nuclear YAP, SOX2 and pSTAT3 in the mesenchynmal-like, vimentin positive PDAC biopsies that we found lack pSMAD2, that were excised from the patients with the shorter medium survival (Fig. 6a, a'). These findings imply that patients with genetic/epigenetic alterations that compromise TGFβ signaling are uniquely mechanically-activated and develop a unique, matricellular-enriched stroma that contributes to their aggression through YAP and SOX2 activation (Fig. 6b). Patients lacking TGFβ signaling may represent a unique cohort of PDACs towards which anti-stromal therapies should be judiciously applied.

Discussion

While PDACs present with inarguably elevated stromal fibrosis, recent findings suggest that collagen abundance may associate with better patient prognosis, with high collagen content correlating with a well-differentiated PDAC phenotype[44,58]. Nevertheless, elevated fibrillar collagen has repeatedly been implicated in both PDAC aggression and treatment resistance[43]. To address these contradictory perspectives, we examined the relationship between tumor genotype, tissue tension, and fibrosis composition and architecture in PDAC progression and aggression.

Using a series of well-characterized GEMMs, we identified a unique matricellular-stromal signature that associates with PDAC genotypes that elevate pancreatic cell contractility and tumor aggression. This coordination of genetically-induced tumor cell contractility and matricellular-enriched fibrosis "tunes" PDAC tissue tension and ultimately activates Yap to promote tumor aggression. This interplay suggests that bulk collagen content is a poor surrogate for the multifacted contributions of PDAC fibrosis to cancer aggression. Specifically, genetically-elevated epithelial tension promoted Yap activation and tumor aggression by stimulating Stat3-mediated ECM remodeling and stiffening of the stroma surrounding the developing pancreatic lesions. Consistently, ectopically-increasing epithelial mechanosignaling induced a matricellular-rich fibrosis and stiffened the stroma adjacent to the pancreatic epithelium, and activated Yap and Stat3 to induce inflammation and accelerate pancreatic transformation and induce aggression. Mechanistically, genetically-increasing epithelial Stat3 activity amplified epithelial tension to drive a matricellular-enriched stiffened phenotype and accelerate malignancy, whereas genetic-ablation of epithelial Stat3 reduced epithelial tension, diminished fibrosis and tempered tumor aggression. Our findings provide the first direct evidence that PDAC genotype calibrates tumor cell contractility to modulate the fibrotic phenotype of the tissue and by so doing modifies the pathology of the resultant cancer.

By exploiting a series of GEMMs, we were able to elucidate that the matricellular-enriched fibrotic phenotype we clinically-linked to the increased tumor cell contractility and loss of TGFβ signaling was driven by a highly conserved JAK/Stat3 cytokine feed forward circuit[50]. We demonstrated, for the first time, that in the absence of TGFβ signaling the Kras transformed tumor epithelium exhibits a significantly elevated actomyosin-mediated tension that is stimulated by an autocrine, cytokine-induced JAK-ROCK-Stat3 mechanosignaling circuit which conditions, remodels and stiffens the ECM adjacent to the developing pancreatic lesions to further amplify pStat3 signaling and drive tumor progression. Our data showed that this feed forward circuit potentiates a Stat3-mediated epithelial pro-inflammatory phenotype and promotes FAK-dependent Yap activation to drive tumor progression and aggression. Indeed, while inflammation and fibrosis can both independently promote pancreatic transformation and aggression, our findings are the first to describe a novel mechanism whereby Stat3-mediated tumor aggression is able to directly induce epithelial contractility to drive ECM stiffening and modify the fibrotic response[51,52]. Of clinical relevance, we demonstrated that nuclear YAP and YAP targets are

progressively increased as a function of PDAC transformation and tissue fibrosis, and we showed that this phenotype is significantly accelerated by Stat3-driven, contractility-mediated tissue stiffening (compare Fig. 2a to Fig. 5f). Our clinical findings revealed that the least differentiated PDACs and the PDACs developing in patients with the shortest survival that lacked TGFβ signaling also had the highest epithelial contractility and expressed elevated pSTAT3, YAP and the YAP target SOX2, all transcriptional regulators that have been implicated in tumor aggression and epithelial-to-mesenchymal transition[31–34]. Indeed, these same YAP and SOX2 expressing tumors also stained strongly for markers of a mesenchymal-like phenotype including vimentin and tenascin C (Fig. 6a, a')[59–61]. Given that YAP signaling can drive Kras-independent PDAC growth and survival, these findings imply that fibrotic PDAC tumors may naturally evolve towards Kras independence and that this phenotype will be potentiated by specific tumor genotypes including loss of TGFβ signaling. Accordingly, these findings may need to be taken into consideration when designing treatment strategies to treat pancreatic cancer patients with drugs such as next generation Ras inhibitors or anti stromal therapies[20,33]. Such results may also provide a rationale for the failures of classic anti-stromal therapies which do not target epithelial-driven fibrosis (NCT01472198)[10–12]. In this regard, our data present one plausible explanation for the mixed response of PDAC cancer patients to anti-stromal therapies, and suggest that FAK and JAK inhibitors, which target both stromal and epithelial-driven fibrosis, and both of which reduced YAP and tenascin induction, may comprise more efficacious therapeutic options.

While the magnitude of the fibrotic response derived from each distinct PDAC genotype initially varied, all of the PDAC models used in our studies eventually trended towards the development of fibrosis, albeit with different end stage fibrotic phenotypes. Thus, although the KPC model demonstrated muted epithelial contractility and initial lower levels of tissue tension compared to the highly fibrotic KTC model, KPC tumor progression was eventually accompanied by an activated stroma that developed into a robust fibrotic response, a progressive stiffening of the ECM and accumulation of high nuclear Yap, in at least a subset of pancreatic tumor cells. The data suggest a primary tumor evolution towards the mesenchymal-like features often observed in patients presenting with recurrent PDAC. In fact, mesenchymal-like PDACs express higher levels and activity of YAP which, in turn, feeds back to further promote a pro-fibrotic, mesenchymal-like tumor phenotype both directly and via stimulation of SOX2. Our

results thereby suggest that patients presenting with high grade PDAC will exhibit a highly mechanoresponsive epithelial phenotype early in PDAC progression while patients presenting with low grade disease will exhibit a gradual elevation of tissue fibrosis leading to eventual YAP activation in the epithelial and stromal compartments by end state PDAC, as well as in recurring tumors. Given that YAP drives an EMT and mesenchymal-like tumor cells exhibit stromally-independent survival and growth, stromal ablation in PDAC patients with pre-existing disease or aggressive genotypes would predictably fail. Thus, our results may explain why ablation of fibrosis does not always block PDAC progression and, in some instances, actually promotes tumor aggression and why recent clinical trials using anti-stromal fibrotic agents failed to provide benefit to patients. Indeed, given that Kras-dependency is strongly linked to epithelial status [62] which diminishes with EMT and that YAP drives PDAC aggression independently of Kras by activating an EMT-like program[33], most PDAC patients may similarly exhibit resistance to targeted therapies including receptor tyrosine kinases and their downstream effectors and new generation Ras therapies. Importantly, our studies suggest that novel treatment modalities holistically targeting both epithelial and stromal-driven fibrosis, cellular contractility and YAP activity, such as combinatory FAK/JAK inhibitor cocktails, will likely prove to be more efficacious therapeutic strategy with which to treat PDAC patients. These observations are consistent with previous implications of YAP in mechanotrasduction[38] and provide a mechanistic rationale with which to design future therapeutic interventions for patients since the highly contractile cell phenotype driven by Stat3 signaling exhibits high YAP activity which is reminiscent of the quasi-mesenchymal-like and recurrent patient PDAC phenotype. Taken together with previous findings, our work would then suggest that the use of FAK inhibitors should provide therapeutic benefit for the quasi-mesenchymal and Kras-independent PDAC subtypes with elevated YAP, block progression and recurrence of low grade PDAC, and slow the progression of high grade PDAC.

Experimental procedures

Human samples

Formalin-fixed, paraffin-embedded human PDAC tissue sections, lacking any patient-identifying information, were commercially purchased from US Biomax (PA961a) or obtained from cohort of patients based on long and short survival [48].

Mice studies

All mice were maintained in accordance with University of California Institutional Animal Care and Use Committee guidelines under protocol number AN105326-01D. Transgenic mouse strains, $Kras^{LSL\text{-}G12D/+}$;Ptf1a-Cre (KC; [49]), $Kras^{LSL\text{-}G12D/+}$;$TGFbR2^{flox/wt\ or\ flox/flox}$;Ptf1a-Cre (KTC; [23]); $Kras^{LSL\text{-}G12D/+}$;$TrP53^{R172H/+}$; Pdx1-Cre (KPC; [24], LSL-β1V737N [54]), $Stat3^{flox/flox}$ [57] and constitutively active Stat3C [56] were described previously. Mice were interbred and maintained in mixed background. Aged matched littermates not expressing Cre as well as Ptf1a-Cre and Pdx1-Cre mice were used as controls.

For FAK inhibition studies, Ptf1a-Cre/β1V737N mice were treated with FAK inhibitor PND-1186 at 0.5 mg/ml in 5% sucrose in the drinking water, control mice were provided 5% sucrose as drinking water (n = 5 per group). Treatment started at 3 weeks and mice were killed after 3 weeks. For JAK inhibition, KTC mice were treated with JAK inhibitor Ruxolitinib twice daily by oral gavage at 60 mg/kg body weight in 0.5% methylcellulose in water. Control mice were provided 0.5% methylcellulose in water (n = 5 per group). Treatment started at 3 weeks and mice were killed after 3 weeks.

For orthotopic xenografts, $5x10^5$ firefly luciferase-mApple expressing cells in Matrigel (BD Biosciences) were injected into the pancreas of 8-week old nude mice (Simonsen laboratory) (n = 5 per group) and tumor growth was monitored by weekly bioluminescent imaging.

For bioluminescent imaging animals were injected intraperitoneally with 3 mg of D-Luciferin and imaged using IVIS spectrum imaging system. The living imaging 4.3 software was used for analysis of the images post acquisition.

Histology

Paraffin-embedded or Fresh frozen pancreatic tissues were analyzed by H&E, picrosirius red, masson's trichrome or alcian blue according to the manufacturer's instructions.

LC-MS/MS and LC-SRM Proteomic analysis

Proteomic analysis was performed in triplicate on 5 milligrams of fresh frozen KC, KPC, and KTC pancreatic tissues as previously described [63] Briefly, tissues were milled in liquid N2

followed by sequential extraction of cellular proteins, soluble ECM proteins, and insoluble ECM proteins. Tryptic digests of all fractions were analyzed by both LC-MS/MS and LC-SRM mass spectrometry. Peptide Spectral Matches (PSMs) from LC-MS/MS was used for relative comparisons of protein abundances between samples. Additionally, Stable Isotope Labeled (SIL) peptides were used for absolute quantification of ECM proteins by LC-SRM.

Atomic force microscopy measurements

Atomic force microscopy and analysis were performed as previously described [64].

Two-photon second harmonics microscopy and image analysis

Two-photon imaging of pancreatic tissues and collagen gels was performed and quantified as previously described [65].

Traction force microscopy

Traction of pancreatic cells was measured as previously described [40,66].

Three dimensional collagen contraction assay

Collagen contraction assay was performed as previously described [50]

Polyacrylamide substrates

Fibronectin conjugated polyacrylamide hydrogels were prepared as previously described [54].

Cytokine antibody array.

Cytokine levels were screened by using mouse cytokine antibody array according to the manufacturer's instructions.

Immunostaining and immunoblotting

Immunofluorescence and immunoblotting analysis were performed as previously described [67]. Antibodies used for immunofluorescence and immunoblotting analysis are listed in the extended experimental procedures.

Lentivirus-mediated shRNA knockdown

Lentiviral shRNA targeting ROCK1 and FAK and nontargeting shRNA control were cloned in the pLKO vector. The TRC IDs for the shRNA used in the study are listed in the extended experimental procedures.

Bioinformatics

Patient expression data was pulled from publicly available dataset GSE21501 obtained from NCBI GEO. Following baseline normalization, expression values for Col1a2, Col2a1, and Col4a1 were used to create a median centroid value representing an average collagen expression

score for each patient. These values were then divided into high and low expression based on median centroid value for the patient set and graphed as survival of each group over time. Kaplan–Meier survival curves were analyzed by Cox–Mantel Log-rank analysis.

Acknowledgments

We thank Dr. M. Dembo for the LIBTRC 2.0 traction force software. Animal handling was supported by L. Korets. This work was supported by US National Institutes of Health NCI grants U01 CA151925-01 (V.M.W., H.L.M. and R.K.), R33 CA183685-01 (V.M.W., K.H.), R01 CA138818-01A1 (V.M.W.), U54CA143836-01 (V.M.W.) and CA102310 (D.D.S.), the Pancreatic Cancer Action Network- AACR Innovative Grant 30-60-25-WEAV (V.M.W.), NSF GRFP 1144247 and NIH/NCI F31CA180422 (Y.A.M.) and NIH TL1 TR001081 (A.S.B).

References

1. Ryan, D. P., Hong, T. S. & Bardeesy, N. Pancreatic Adenocarcinoma. *N*. *Engl*. *J*. *Med*. **371,** 1039–1049 (2014).

2. Chauhan, V. P. *et al*. Compression of pancreatic tumor blood vessels by hyaluronan is caused by solid stress and not interstitial fluid pressure. *Cancer Cell* **26,** 14–5 (2014).

3. Swartz, M. A. & Lund, A. W. Lymphatic and interstitial flow in the tumour microenvironment: linking mechanobiology with immunity. *Nat*. *Rev*. *Cancer* **12,** 210–219 (2012).

4. Yu, M. & Tannock, I. F. Targeting Tumor Architecture to Favor Drug Penetration: A New Weapon to Combat Chemoresistance in Pancreatic Cancer? *Cancer Cell* **21,** 327–329 (2012).

5. Provenzano, P. P. & Hingorani, S. R. Hyaluronan, fluid pressure, and stromal resistance in pancreas cancer. *Br*. *J*. *Cancer* **108,** 1–8 (2013).

6. Neesse, A., Krug, S., Gress, T. M., Tuveson, D. A. & Michl, P. Emerging concepts in pancreatic cancer medicine: Targeting the tumor stroma. *Onco*. *Targets*. *Ther*. **7,** 33–43 (2013).

7. Olive, K. P. *et al*. Inhibition of Hedgehog signaling enhances delivery of chemotherapy in a mouse model of pancreatic cancer. *Science* **324,** 1457–1461 (2009).

8. Provenzano, P. P. *et al*. Enzymatic targeting of the stroma ablates physical barriers to treatment of pancreatic ductal adenocarcinoma. *Cancer Cell* **21,** 418–29 (2012).

9. Chauhan, V. P. *et al*. Angiotensin inhibition enhances drug delivery and potentiates chemotherapy by decompressing tumour blood vessels. *Nat*. *Commun*. **4,** 2516 (2013).

10. Rosow, D. E. *et al*. Sonic Hedgehog in pancreatic cancer: from bench to bedside, then back to the bench. *Surgery* **152,** S19–32 (2012).

11. Ozdemir, B. C. *et al*. Depletion of carcinoma-associated fibroblasts and fibrosis induces immunosuppression and accelerates pancreas cancer with reduced survival. *Cancer Cell* **25,** 719–34 (2014).

12. Rhim, A. D. *et al*. Stromal elements act to restrain, rather than support, pancreatic ductal adenocarcinoma. *Cancer Cell* **25,** 735–47 (2014).

13. Pickup, M. W., Mouw, J. K. & Weaver, V. M. The extracellular matrix modulates the hallmarks of cancer. *EMBO Rep*. **15,** 1243–1253 (2014).

14. Butcher, D. T., Alliston, T. & Weaver, V. M. A tense situation: forcing tumour progression. *Nat*. *Rev*. *Cancer* **9,** 108–122 (2009).

15. Cheung, K. J., Gabrielson, E., Werb, Z. & Ewald, A. J. Collective invasion in breast cancer requires a conserved basal epithelial program. *Cell* **155,** 1639–1651 (2013).

16. Hoadley, K. A. *et al*. Multiplatform Analysis of 12 Cancer Types Reveals Molecular Classification within and across Tissues of Origin. *Cell* (2013). doi:10.1016/j.cell.2014.06.049

17. Thiery, J. P., Acloque, H., Huang, R. Y. J. & Nieto, M. A. Epithelial-Mesenchymal Transitions in Development and Disease. *Cell* **139,** 871–890 (2009).

18. Collisson, E. a. *et al*. Comprehensive molecular profiling of lung adenocarcinoma. *Nature* **511,** 543–50 (2014).

19. Collisson, E. a *et al*. Subtypes of pancreatic ductal adenocarcinoma and their differing responses to therapy. *Nat*. *Med*. **17,** 500–3 (2011).

20. Kapoor, A. *et al*. Yap1 activation enables bypass of oncogenic kras addiction in pancreatic cancer. *Cell* **158,** 185–97 (2014).

21. Deer, E. L. *et al*. Phenotype and genotype of pancreatic cancer cell lines. *Pancreas* **39,** 425–435 (2010).

22. Pérez-Mancera, P. A., Guerra, C., Barbacid, M. & Tuveson, D. A. What we have learned about pancreatic cancer from mouse models. *Gastroenterology* **142,** 1079–1092 (2012).

23. Ijichi, H. *et al*. Aggressive pancreatic ductal adenocarcinoma in mice caused by pancreas-specific blockade of transforming growth factor-β signaling in cooperation with active Kras expression. *Genes Dev*. **20,** 3147–3160 (2006).

24. Hingorani, S. R. *et al*. Trp53R172H and KrasG12D cooperate to promote chromosomal instability and widely metastatic pancreatic ductal adenocarcinoma in mice. *Cancer Cell* **7,** 469–483 (2005).

25. Aguirre, A. J. *et al*. Activated Kras and Ink4a/Arf deficiency cooperate to produce metastatic pancreatic ductal adenocarcinoma. *Genes Dev*. **17,** 3112–3126 (2003).

26. Bardeesy, N. *et al*. Smad4 is dispensable for normal pancreas development yet critical in progression and tumor biology of pancreas cancer. *Genes Dev*. **20,** 3130–3146 (2006).

27. Kabashima, A. *et al*. Side population of pancreatic cancer cells predominates in TGF-beta-mediated epithelial to mesenchymal transition and invasion. *Int*. *J*. *Cancer* **124,** 2771–2779 (2009).

28. Izeradjene, K. *et al*. KrasG12D and Smad4/Dpc4 Haploinsufficiency Cooperate to Induce Mucinous Cystic Neoplasms and Invasive Adenocarcinoma of the Pancreas. *Cancer Cell* **11,** 229–243 (2007).

29. Izumchenko, E. *et al*. The TGFβ-miR200-MIG6 pathway orchestrates the EMT-associated kinase switch that induces resistance to EGFR inhibitors. *Cancer Res*. **74,** 3995–4005 (2014).

30. Rhim, A. D. *et al*. EMT and dissemination precede pancreatic tumor formation. *Cell* **148,** 349–361 (2012).

31. Herreros-Villanueva, M. *et al*. SOX2 promotes dedifferentiation and imparts stem cell-like features to pancreatic cancer cells. *Oncogenesis* **2,** e61 (2013).

32. Jiang, J. *et al*. MiR-1181 inhibits stem cell-like phenotypes and suppresses SOX2 and STAT3 in human pancreatic cancer. *Cancer Lett*. **356,** 962–970 (2015).

33. Shao, D. D. *et al*. KRAS and YAP1 converge to regulate EMT and tumor survival. *Cell* **158,** 171–184 (2014).

34. Yimlamai, D. *et al*. Hippo pathway activity influences liver cell fate. *Cell* **157,** 1324–1338 (2014).

35. Zhang, J. *et al*. YAP-dependent induction of amphiregulin identifies a non-cell-autonomous component of the Hippo pathway. *Nat*. *Cell Biol*. **11,** 1444–1450 (2009).

36. Seo, E. *et al*. SOX2 Regulates YAP1 to Maintain Stemness and Determine Cell Fate in the Osteo-Adipo Lineage. *Cell Rep*. **3,** 2075–2087 (2013).

37. Basu-roy, U. *et al*. Sox2 antagonizes the Hippo pathway to maintain stemness in cancer cells. *Nat*. *Commun*. **6,** 1–14 (2015).

38. Dupont, S. *et al*. Role of YAP/TAZ in mechanotransduction. *Nature* **474,** 179–183 (2011).

39. Yu, F. X. *et al*. Regulation of the Hippo-YAP pathway by G-protein-coupled receptor signaling. *Cell* **150,** 780–791 (2012).

40. Paszek, M. J. *et al*. Tensional homeostasis and the malignant phenotype. *Cancer Cell* **8,** 241–254 (2005).

41. Calvo, F. *et al*. Mechanotransduction and YAP-dependent matrix remodelling is required for the generation and maintenance of cancer-associated fibroblasts. *Nat Cell Biol* **15,** 637–646 (2013).

42. Samuel, M. S. *et al*. Actomyosin-mediated cellular tension drives increased tissue stiffness and β-catenin activation to induce epidermal hyperplasia and tumor growth. *Cancer Cell* **19,** 776–791 (2011).

43. Erkan, M. *et al*. The Activated Stroma Index Is a Novel and Independent Prognostic Marker in Pancreatic Ductal Adenocarcinoma. *Clin*. *Gastroenterol*. *Hepatol*. **6,** 1155–1161 (2008).

44. Sinn, M. *et al*. α-Smooth muscle actin expression and desmoplastic stromal reaction in pancreatic cancer: results from the CONKO-001 study. *Br*. *J*. *Cancer* **111,** 1917–1923 (2014).

45. Bever, K. M. *et al*. The prognostic value of stroma in pancreatic cancer in patients receiving adjuvant therapy. *Hpb* n/a–n/a (2014). doi:10.1111/hpb.12334

46. Dangi-Garimella, S. *et al*. Three-dimensional collagen I promotes gemcitabine resistance in pancreatic cancer through MT1-MMP-mediated expression of HMGA2. *Cancer Res*. **71,** 1019–1028 (2011).

47. Wang, W. Q. *et al*. Intratumoral α-SMA Enhances the Prognostic Potency of CD34 Associated with Maintenance of Microvessel Integrity in Hepatocellular Carcinoma and Pancreatic Cancer. *PLoS One* **8,** (2013).

48. Schultz, N. a *et al*. MicroRNA biomarkers in whole blood for detection of pancreatic cancer. *JAMA* **311,** 392–404 (2014).

49. Hingorani, S. R. *et al*. Preinvasive and invasive ductal pancreatic cancer and its early detection in the mouse. *Cancer Cell* **4,** 437–450 (2003).

50. Sanz-Moreno, V. *et al*. ROCK and JAK1 Signaling Cooperate to Control Actomyosin Contractility in Tumor Cells and Stroma. *Cancer Cell* **20,** 229–245 (2011).

51. Fukuda, A. *et al*. Stat3 and MMP7 Contribute to Pancreatic Ductal Adenocarcinoma Initiation and Progression. *Cancer Cell* **19,** 441–455 (2011).

52. Lesina, M. *et al*. Stat3/Socs3 Activation by IL-6 Transsignaling Promotes Progression of Pancreatic Intraepithelial Neoplasia and Development of Pancreatic Cancer. *Cancer Cell* **19,** 456–469 (2011).

53. Ijichi, H. *et al*. Inhibiting Cxcr2 disrupts tumor-stromal interactions and improves survival in a mouse model of pancreatic ductal adenocarcinoma. *J*. *Clin*. *Invest*. **121,** 4106–4117 (2011).

54. Mouw, J. K. *et al*. Tissue mechanics modulate microRNA-dependent PTEN expression to regulate malignant progression. *Nat*. *Med*. **20,** 360–7 (2014).

55. Li, R. *et al*. Activation of integrin alphaIIbbeta3 by modulation of transmembrane helix associations. *Science* **300,** 795–798 (2003).

56. Barbieri, I. *et al*. Constitutively active Stat3 enhances neu-mediated migration and metastasis in mammary tumors via upregulation of Cten. *Cancer Res*. **70,** 2558–2567 (2010).

57. Musteanu, M. *et al*. Stat3 Is a Negative Regulator of Intestinal Tumor Progression in ApcMin Mice. *Gastroenterology* **138,** (2010).

58. Whatcott, C. J. *et al*. Desmoplasia in primary tumors and metastatic lesions of pancreatic cancer. *Clin*. *Cancer Res*. (2015). doi:10.1158/1078-0432.CCR-14-1051

59. Kohler, I. *et al*. Detailed analysis of epithelial-mesenchymal transition and tumor budding identifies predictors of long-term survival in pancreatic ductal adenocarcinoma. *J*. *Gastroenterol*. *Hepatol*. **30,** 78–84 (2015).

60. Paron, I. *et al*. Tenascin-c enhances pancreatic cancer cell growth and motility and affects cell adhesion through activation of the integrin pathway. *PLoS One* **6,** (2011).

61. Esposito, I. *et al*. Tenascin C and annexin II expression in the process of pancreatic carcinogenesis. *J*. *Pathol*. **208,** 673–685 (2006).

62. Singh, A. *et al*. A Gene Expression Signature Associated with 'K-Ras Addiction' Reveals Regulators of EMT and Tumor Cell Survival. *Cancer Cell* **15,** 489–500 (2009).

63. Hill, R. C., Calle, E. a., Dzieciatkowska, M., Niklason, L. E. & Hansen, K. C. Quantification of Extracellular Matrix Proteins from a Rat Lung Scaffold to Provide a Molecular Readout for Tissue Engineering. *Mol*. *Cell*. *Proteomics* **14,** 961–973 (2015).

64. Lopez, J. I., Kang, I., You, W.-K., McDonald, D. M. & Weaver, V. M. In situ force mapping of mammary gland transformation. *Integr*. *Biol*. *(Camb)*. **3,** 910–921 (2011).

65. Pickup, M. W. *et al*. Stromally derived lysyl oxidase promotes metastasis of transforming growth factor-??-deficient mouse mammary carcinomas. *Cancer Res*. **73,** 5336–5346 (2013).

66. Reinhart-King, C. A., Dembo, M. & Hammer, D. A. Endothelial cell traction forces on RGD-derivatized polyacrylamide substrata. *Langmuir* **19,** 1573–1579 (2003).

67. Paszek, M. J. *et al*. The cancer glycocalyx mechanically primes integrin-mediated growth and survival. *Nature* **511,** 319–25 (2014).

Figure Legends

Figure 1: Human PDAC aggression is characterized by low epithelial TGFβ signaling and high myosin activity.

(a) Kaplan-Meier of overall survival of PDAC patients from GSE21501 with patients divided into those with high and low collagen expression by normalized microarray analysis of collagen gene expression, log rank p=0.04, n=67. **(b)** Representative photomicrographs of H&E (top panel) and Masson's Trichrome (2nd panel) stained PDAC tissue arrays from patients with well (n=19), moderately (n=23) or poorly differentiated (n=26) tumors. Scale bar, 100μm. Representative immunofluorescence images of pancreatic tissue described above stained for αSMA (red, 3rd, panel), pMLC2 (red, 7th panel), pSMAD2 (red, 8th panel) and DAPI (blue). Scale bar, 75μm. Representative polarized light images of picrosirius red (PR) stained pancreatic tissue (as described above) revealing collagen fiber structure, orientation and distribution within the tissue stroma (4th panel). Scale bar, 50μm. Representative second harmonic generation (SHG) images of extracellular collagen architecture in the pancreatic tissue around the epithelial ductal region described above (5th panel) and SHG color-coded images revealing collagen fiber diameter (6th panel). Scale bar, 75μm. **(b')** Bar graphs quantifying the tissue images shown in the panels in b. **(c)** Representative photomicrographs of H&E (top panel) and Masson's Trichrome (2nd panel) stained PDAC tissue arrays from PDAC patients cohort representing patients with a median short survival of 11-289 days (n=29) and median long survival of 1090-3298 days (n=28). Scale bar, 100μm. Representative immunofluorescence images of pancreatic tissue (as described above) stained for αSMA (red, 3rd, panel), pMLC2 (red, 7th panel), pSMAD2 (red, 8th panel) and DAPI (blue). Scale bar, 75μm. Representative polarized light images of PR stained pancreatic tissue as described above revealing collagen fiber structure, orientation and distribution within the tissue stroma (4th panel). Scale bar, 50μm. Representative SHG images of extracellular collagen architecture in the pancreatic tissue around the epithelial ductal region described above (5th panel) and SHG color-coded images revealing collagen fiber diameter (6th panel). Scale bar, 75μm. **c'.** Bar graphs quantifying the tissue images shown in the panels in c. (*p<0.05; **p<0.01, ***p<0.001, ****p<0.0001, "ns" denotes not significant).

Figure 2: Tumor genotype tunes epithelial tension to regulate the fibrotic phenotype.

(a) Representative SHG images of extracellular collagen architecture and distribution in the pancreatic tissue from 20 weeks old pancreatic tissue excised from mice expressing Kras (KC), Kras with one mutant allele of P53 (KPC) or Kras with heterozygous loss of Tgfr2 in the pancreatic epithelium (KTC) (1st panel). Scale bar, 75µm.Representative force maps measured using AFM indentation of the stiffness of the extracellular matrix surrounding the pancreatic ductal lesions developing in the 20 week old animals (1st panel insert). Representative immunofluorescence images of pancreatic tissue described above stained for Tenascin C (red, 2nd panel; scale bar, 75µm), pMLC2 (red, 3rd panel), β1integrin/pFAK (green/red, 4th panel), pMyPT1 (red, 5th panel), YAP (red, 6th panel) and DAPI (blue). Scale bar, 50µm. **(a')** Bar graphs quantifying the fibril thickness and distribution imaged by SHG around the developing pancreatic ductal lesions pf pancreatic tissue described above. **(a")** Bar graphs showing the distribution of the stiffness measurements of the extracellular matrix surrounding the normal and developing lesions (in tissue described above) as assessed by atomic force microscopy indentation. **(b)** Bar graphs quantifying the matrix protein concentration of Tenascin C, Fibronectin 1 and type 12A1 Collagen in tissue described above as measured by mass spectrometry. **(c)** Representative traction force maps measured on polyacrylamide gels (2300 Pa) for isolated KC, KPC and KTC pancreatic epithelial tumor cells. **(c')** Corresponding quantification of c. **(d)** Polarized light images of color-coded PR stained collagen gels incubated with KC, KPC or KTC pancreatic epithelial tumor cells or with KTC cells treated with vehicle or the ROCK inhibitor Y27632. **(d')** Bar graphs quantifying three dimensional collagen gel contraction as indicated by collagen gel area. Cultures were assayed after 24 hours. **(e)** Representative polarized light images of PR stained pancreatic tissue excised from nude mice 3 weeks after injection with KC, KPC, and KTC pancreatic tumor cells expressing either a control shRNA or an shRNA to ROCK (top panel). Scale bar, 75µm. Representative immunofluorescence images of pancreatic tissue described above stained for YAP (red) and DAPI (blue). Scale bar, 50µm (bottom panel). **(e')** Bar graph quantifying the stiffness of the pancreatic tissue shown above in e using AFM indentation. **(e")** Graphs quantifying the total level of fibrillar collagen measured in the pancreatic tissue shown in e. For *in vitro* bar graphs, results are the mean +/- SEM of at least 3 independent experiments. For *in vivo* experiments, N=5 mice per group. (*$p<0.05$; **$p<0.01$, ***$p<0.001$, ****$p<0.0001$, "ns" denotes not significant).

Figure 3: Loss of TGFβ signaling activates a JAK/Stat3 contractility feed forward circuit to induce ECM remodeling and tissue stiffening.

(a) Representative immunofluorescence images of pancreatic tissue excised from 20 week old KC, KPC and KTC mice stained for pStat3 (red) and DAPI (blue). Scale bar, 50μm. **(a')** Bar graphs quantifying the level of stromal versus epithelial p-Stat3 in the tissues stained in a. **(b)** Representative immunofluorescence images of isolated KC, KPC and KTC tumor cells stained for pStat3 (red) and DAPI (blue). Scale bar, 25μm. **(c)** Representative polarized light images of PR stained color-coded fibrillar collagen in three dimensional collagen gels incubated with KTC tumor cells for 24 hours either with vehicle or the JAK inhibitor Ruxolitinib. **(c')** Bar graphs showing amount of collagen contraction as measured by total collagen gel area. **(c")** Bar graphs showing mean collagen fiber diameter measured in the three dimensional collagen gels shown in c. **(d.)** Representative immunoblot of Stat3 activation (pStat3) as a function of time following exposure to the conditioned media (CM) obtained from KTC tumor cells. **(d')** Line graph quantifying the relative level of pStat3 measured in the KC cells shown above in d. **(e)** Representative polarized light images of PR stained, color-coded fibrillar collagen in three-dimensional collagen gels incubated with KC tumor cells treated with vehicle or the conditioned media from 48 hour cultured KTC tumor cells. **(e')** Bar graphs showing amount of collagen contraction as measured by total collagen gel area in e'. **(e")** Bar graphs showing mean collagen fiber diameter measured in the three dimensional collagen gels shown in e. **(f)** Representative immunoblot of total (Stat3) and activated Stat3 (pStat3) levels in KC tumor cells cultured on soft or stiff polyacrylamide substrates. Results are normalized to total Stat3 and Gapdh. **(f')** bar graphs showing quantification of f. **(g)** Quantification of cytokine protein expression measured in the conditioned media of KC cells cultured on soft or soft polyacrylamide substrates. For *in vitro* bar graphs, results are the mean +/- SEM of at least 3 independent experiments. For *in vivo* experiments, N=5 mice per group. (*$p<0.05$; **$p<0.01$, ***$p<0.001$, ****$p<0.0001$, "ns" denotes not significant).

Figure 4: Stat3 induces tissue fibrosis to accelerate Kras-induced PDAC.

(a) Cartoon of mouse manipulations used to study the impact of increasing pancreatic epithelial cell mechanosignaling using β1V737N on Kras-induced pancreatic malignancy. **(b)**

Representative immunofluorescence images of pancreatic tissues excised from 3 month old KC and KC/β1V737N mice stained for p397FAK (top panel; red) and p-MLC2 (2nd panel; red), Tenascin C (5th panel, red), YAP (6th panel, red), pStat3 (7th panel; red), scale bar, 50 μm, CD68 (8th panel; red), and DAPI (blue). Scale bar, 100μm. (3rd panel) Representative polarized light images of collagen fibers revealed by PR staining of pancreatic tissue described above. Scale bar, 75μm. b. (4th panel) Representative force maps of ECM stiffness measured using atomic force microscopy indentation in pancreatic tissue described above. **(b')** Bar graphs quantifying the tissue images shown in the panels in b. **(c)** Representative alcian blue images of transformed ducts and representative H&E images of pancreatic tissue and tumor morphology. Scale bar, 100μm. **c'** corresponding quantification of c. **(d)** Bar graphs showing mouse body weight at study termination. **(e)** (top) Representative polarized light images of collagen fibers revealed by PR staining of pancreatic tissues in nude mice injected with KTC tumor cells expressing either a control shRNA or a FAK shRNA. Scale bar, 75 μm (top panel). Representative immunofluorescence confocal images of pancreatic tissue described above in e stained for pStat3 (red, 2nd panel; scale bar, 25 μm), YAP (red 3rd panel; scale bar, 75 μm) and DAPI (blue). **(e')** Bar graphs quantifying total collagen fibril content of picrosirius stained tissue shown in e. **(e")** Bar graphs quantifying average elastic modulus (Pa) measured by atomic force microscopy of pancreatic tissue shown in e. For *in vivo* experiments, N=5 mice per group. (*$p<0.05$; **$p<0.01$, ***$p<0.001$, ****$p<0.0001$, "ns" denotes not significant).

Figure 5: Stat3 induces tissue fibrosis to accelerate Kras-induced PDAC.

(a) Cartoon depicting the mouse crosses used for the activated Stat3C manipulations. **(b)** Representative immunofluorescence images of pancreatic tissues excised from 5 week old KC and KC/Stat3C mice stained for pStat3 (top panel; red), scale bar, 75 μm, p397FAK (2nd panel; red) and pMLC2 (3rd panel; red), Scale bar, 50 μm, CD68 (5th panel; red), and DAPI (blue). Scale bar, 100μm. b. (4th panel) Representative polarized light images of collagen fibers revealed by PR staining of pancreatic tissue described above. Scale bar, 75μm. b. (7th panel) Representative phase contrast images of H&E stained pancreatic tissue as described above. Scale bar, 100μm. b' Bar graphs quantifying the tissue images shown in the panels in b. **(c)** Kaplan-Meier graph showing survival of KC, Stat3C, and KC/Stat3C mice. **(d)** Quantification of ECM stiffness measured by atomic force microscopy in pancreatic tissue shown in b. **(e)** Cartoon

depicting the mouse crosses used for the Stat3 knock studies. **(f)** Representative immunofluorescence images of pancreatic tissues excised from 5 week old 5 week old homozygous KTC (KTC KO) (Control) and KTC/Stat3 KO mice (Stat3 KO) stained for pStat3 (top panel; red), scale bar, 75 μm, p-397FAK (2nd panel; red) and p-MLC2 (3rd panel; red), scale bar, 50 μm, Tenascin (5th panel; red), CD68 (6th panel; red), scale bar, 100μm, YAP (7th panel; red) scale bar, 50μm, and DAPI (blue). (f) (4th panel) Representative polarized light images of collagen fibers revealed by PR staining of pancreatic tissue described above. Scale bar, 75μm. (f) (8th panel) Representative phase contrast images of H&E stained pancreatic tissue as described above. Scale bar, 100μm. f' Bar graphs quantifying the tissue images shown in the panels in f. **(g)** Kaplan-Meier graph showing survival of KTC and KTC/Stat3 KO mice. **(h)** Quantification of ECM stiffness measured by atomic force microscopy in pancreatic tissue shown in f. For *in vivo* experiments, N=5 mice per group. (*p<0.05; **p<0.01, ***p<0.001, ****p<0.0001, "ns" denotes not significant).

Figure 6: Stat3 enhances epithelial contractility to induce PDAC matricellular fibrosis and tumor aggression to compromise patient survival.

(a) Representative photomicrographs of H&E from PDAC patients cohort representing patients with a median short survival of 11-289 days (n=29) and median long survival of 1090-3298 days (n=28) (top panel). Scale bar, 100μm. Representative SHG images of extracellular collagen architecture in the pancreatic tissue around the epithelial ductal region in tissue described above (2nd panel). Scale bar, 75μm. Representative immunofluorescence images of pancreatic tissue described above stained for Tenascin C (red, 3rd panel), pSMAD2 (red, 4th, panel), pStat3 (red, 5th panel), YAP (red, 6th panel), Sox2 (red, 7th panel), Vimentin (red, 8th panel) and DAPI (blue). Scale bar, 75μm. **(a')** Bar graphs quantifying the tissue images shown in the panels in a. **(b)** Cartoon depicting the epithelial JAK-ROCK-Stat3-YAP feed forward circuit and its potentiation by a stiff extracellular matrix microenvironment.

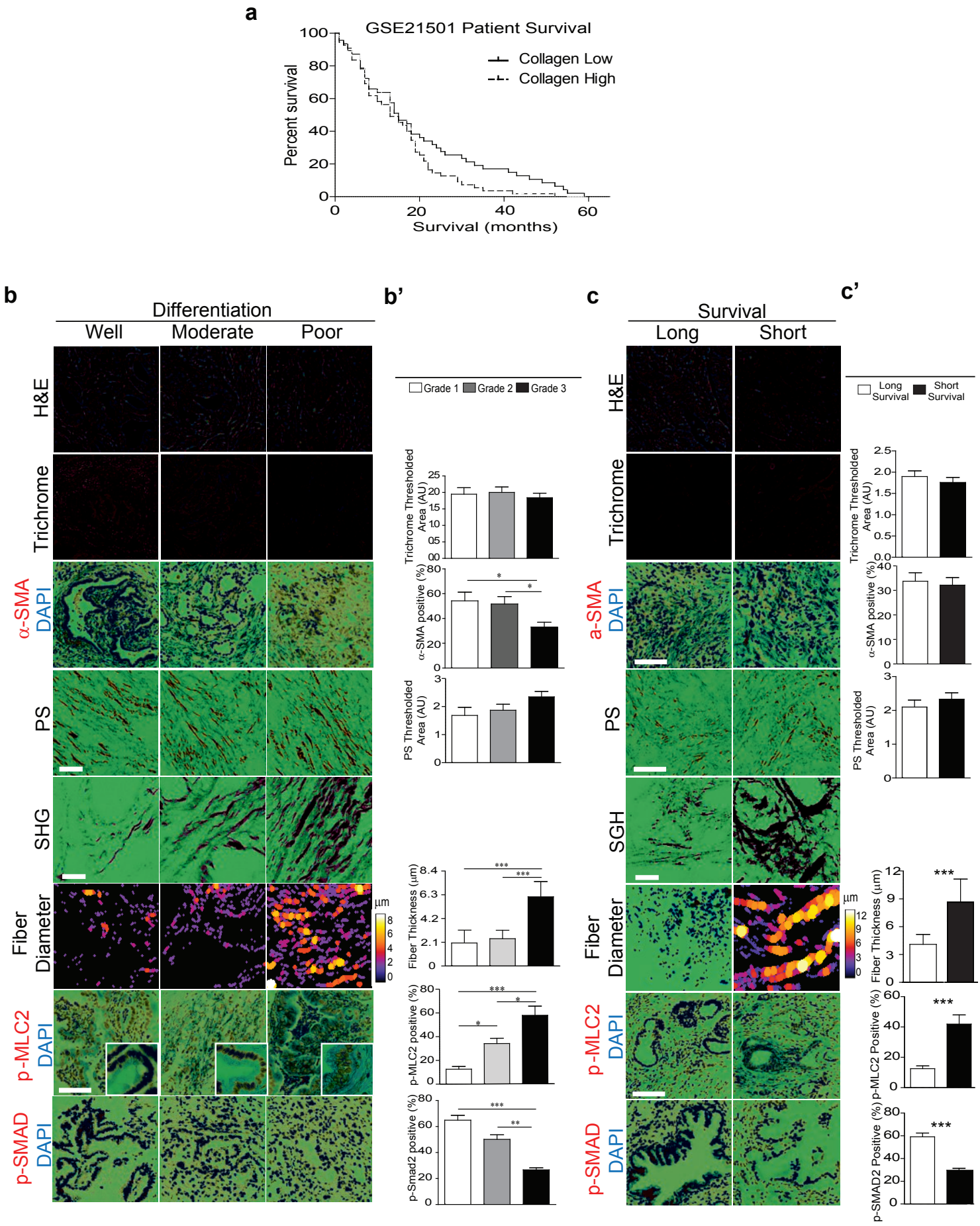
a
GSE21501 Patient Survival
Collagen Low
Collagen High
Percent survival
Survival (months)
b
Differentiation
Well
Moderate
Poor
H&E
Trichrome
α-SMA
DAPI
PS
SHG
Fiber Diameter
p-MLC2
DAPI
p-SMAD
DAPI
µm
b'
Grade 1
Grade 2
Grade 3
Trichrome Thresholded Area (AU)
α-SMA positive (%)
PS Thresholded Area (AU)
Fiber Thickness (µm)
p-MLC2 positive (%)
p-Smad2 positive (%)
c
Survival
Long
Short
H&E
Trichrome
a-SMA
DAPI
PS
SGH
Fiber Diameter
p-MLC2
DAPI
p-SMAD
DAPI
µm
c'
Long Survival
Short Survival
Trichrome Thresholded Area (AU)
α-SMA positive (%)
PS Thresholded Area (AU)
Fiber Thickness (µm)
p-MLC2 Positive (%)
p-SMAD2 Positive (%)

figure 1

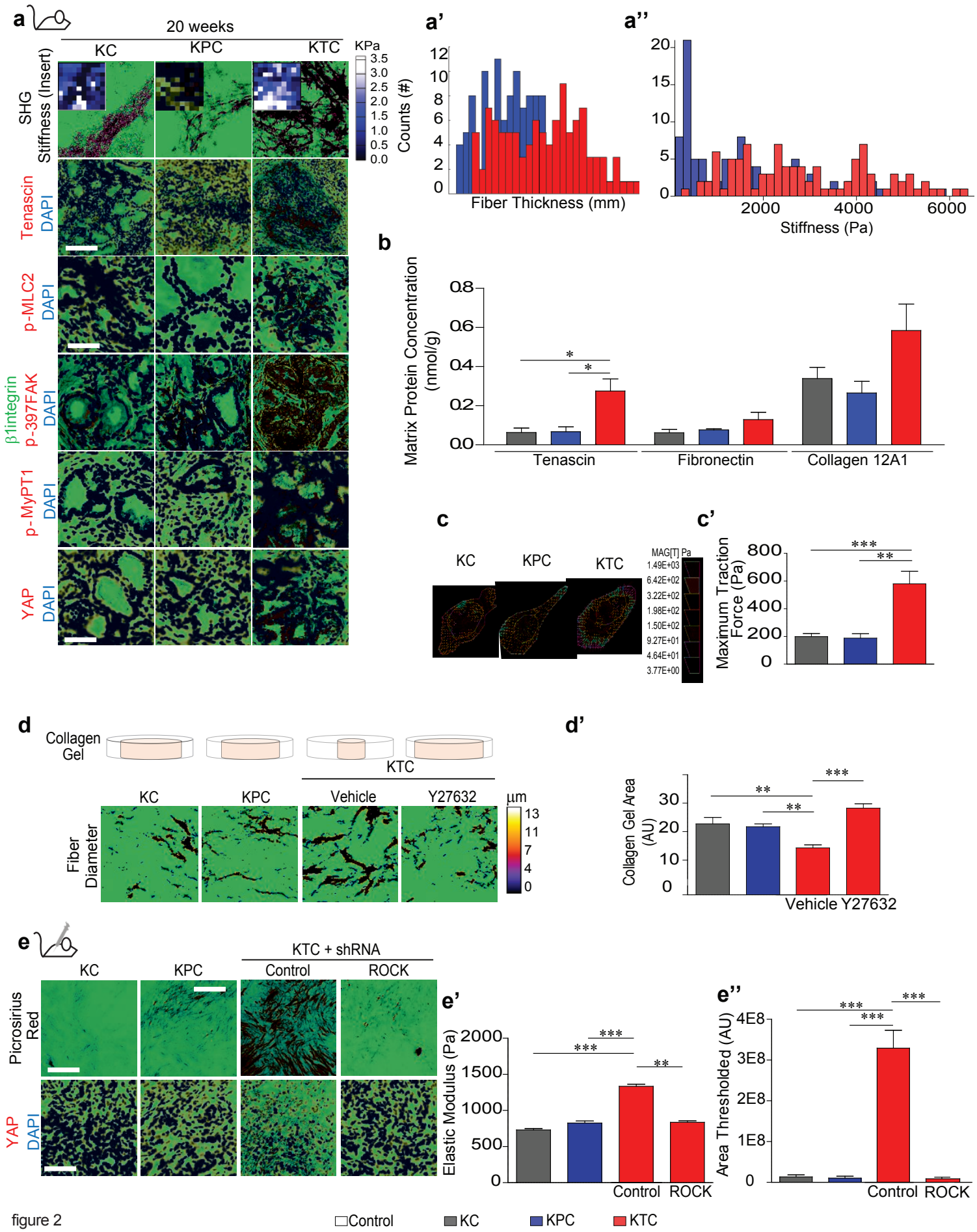
a
20 weeks
KC
KPC
KTC
KPa
3.5
3.0
2.5
2.0
1.5
1.0
0.5
0.0
SHG
Stiffness (Insert)
Tenascin
DAPI
p-MLC2
DAPI
β1integrin
p-397FAK
DAPI
p-MyPT1
DAPI
YAP
DAPI
a'
Counts (#)
Fiber Thickness (mm)
a''
Stiffness (Pa)
b
Matrix Protein Concentration (nmol/g)
Tenascin
Fibronectin
Collagen 12A1
c
MAG[T] Pa
c'
Maximum Traction Force (Pa)
d
Collagen Gel
KTC
KC
KPC
Vehicle
Y27632
Fiber Diameter
μm
d'
Collagen Gel Area (AU)
Vehicle Y27632
e
KTC + shRNA
KC
KPC
Control
ROCK
Picrosirius Red
YAP
DAPI
e'
Elastic Modulus (Pa)
Control
ROCK
e''
Area Thresholded (AU)
Control
ROCK
Control
KC
KPC
KTC

figure 2

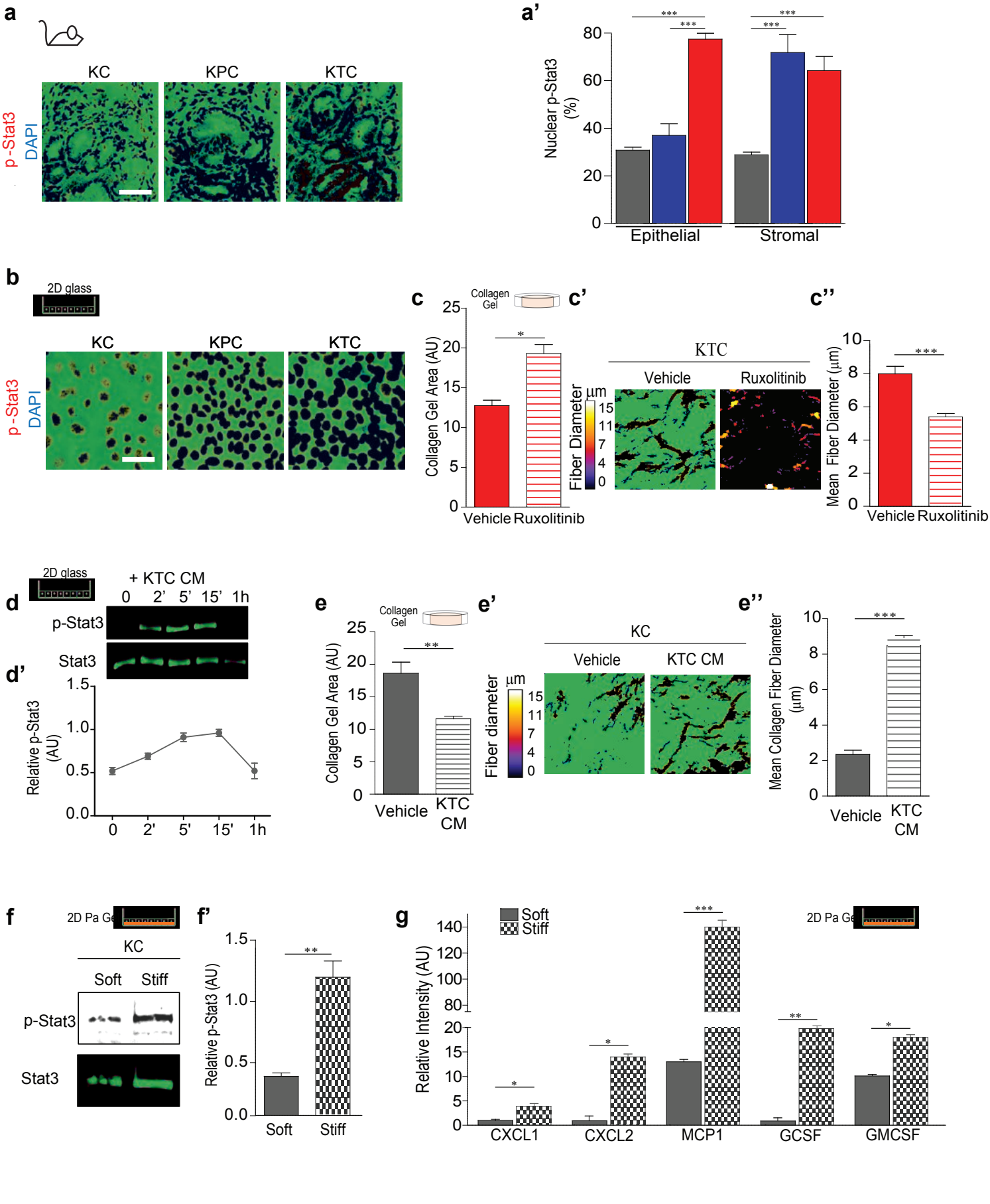
a
KC
KPC
KTC
p-Stat3
DAPI
a'
Nuclear p-Stat3 (%)
Epithelial
Stromal
b
2D glass
c
Collagen Gel
Collagen Gel Area (AU)
Vehicle
Ruxolitinib
c'
KTC
Vehicle
Ruxolitinib
Fiber Diameter
µm
c''
Mean Fiber Diameter (µm)
d
+ KTC CM
0 2' 5' 15' 1h
p-Stat3
Stat3
d'
Relative p-Stat3 (AU)
e
e'
KC
KTC CM
Fiber diameter
e''
Mean Collagen Fiber Diameter (µm)
f
2D Pa Ge
Soft
Stiff
f'
Relative p-Stat3 (AU)
g
Relative Intensity (AU)
CXCL1
CXCL2
MCP1
GCSF
GMCSF
Control
KC
KPC
KTC

figure 3

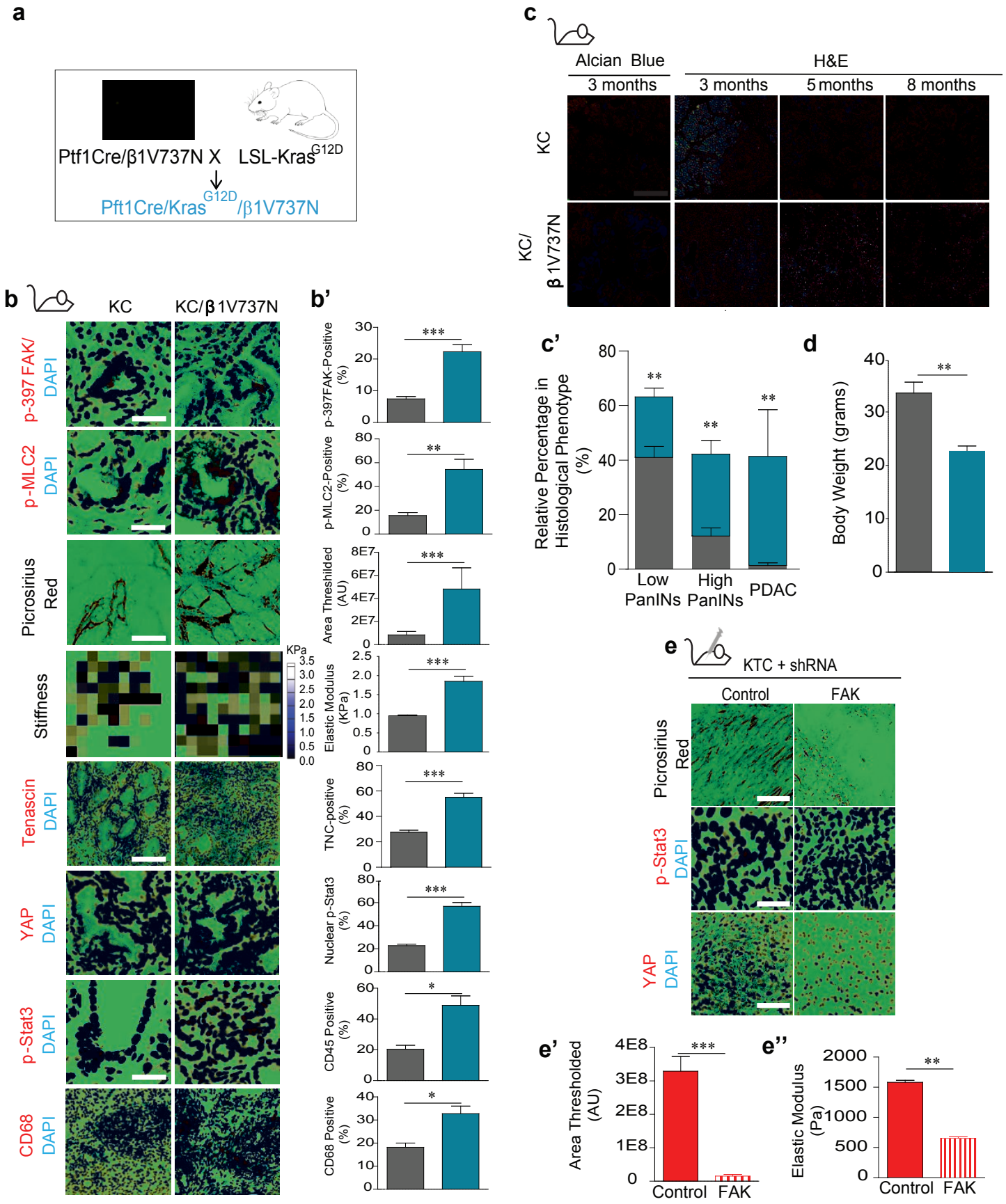
a
Ptf1Cre/β1V737N X LSL-Kras G12D
Pft1Cre/Kras G12D /β1V737N
b
KC
KC/β1V737N
p-397 FAK/ DAPI
p-MLC2 DAPI
Picrosirius Red
Stiffness
KPa
Tenascin DAPI
YAP DAPI
p-Stat3 DAPI
CD68 DAPI
b'
p-397FAK-Positive (%)
p-MLC2-Positive (%)
Area Thresholded (AU)
Elastic Modulus (KPa)
TNC-positive (%)
Nuclear p-Stat3 (%)
CD45 Positive (%)
CD68 Positive (%)
c
Alcian Blue
H&E
3 months
3 months
5 months
8 months
KC
KC/ β1V737N
c'
Relative Percentage in Histological Phenotype (%)
Low PanINs
High PanINs
PDAC
d
Body Weight (grams)
e
KTC + shRNA
Control
FAK
Picrosirius Red
p-Stat3 DAPI
YAP DAPI
e'
Area Thresholded (AU)
e''
Elastic Modulus (Pa)
KC
KC/β1V737N
KTC

figure 4

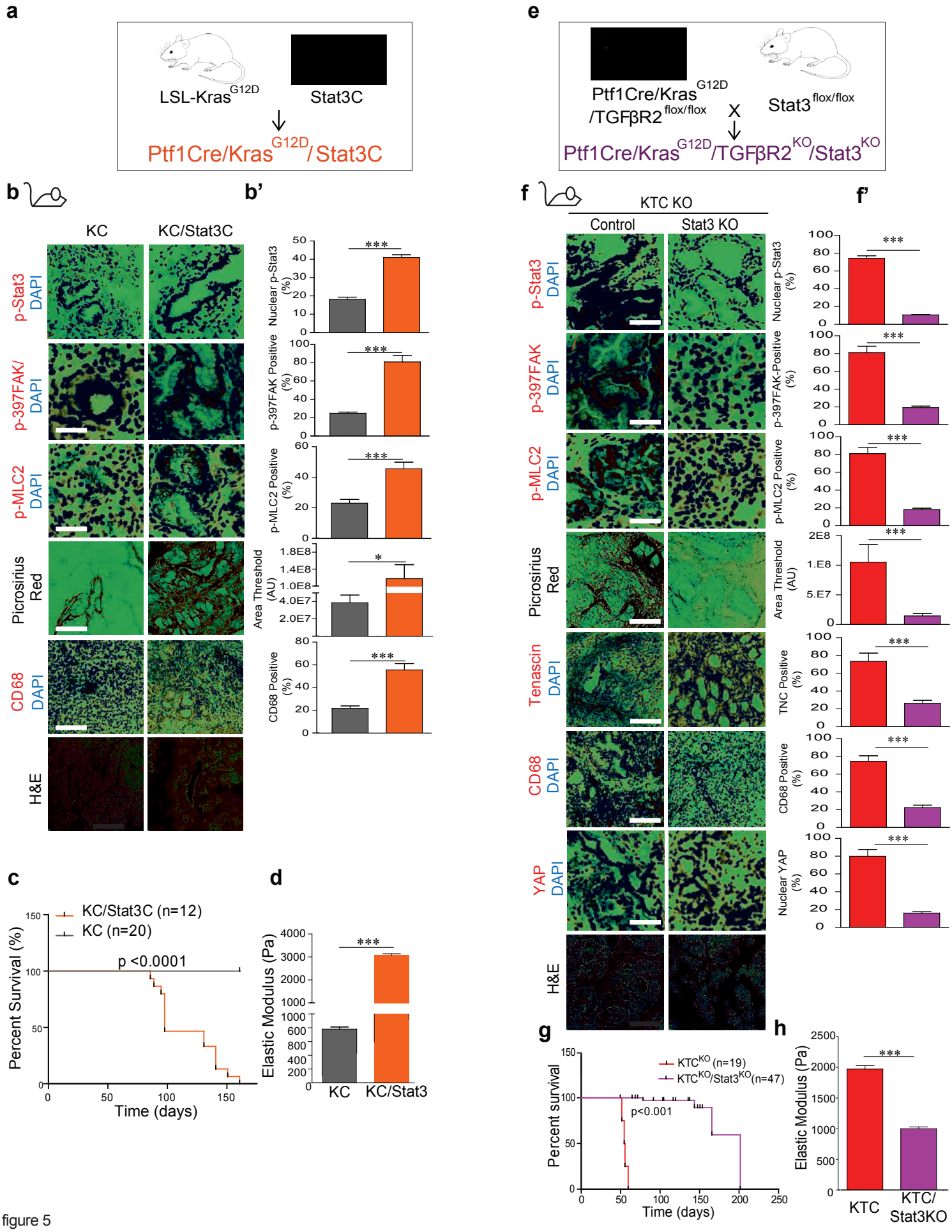
a
LSL-Kras G12D
Stat3C
Ptf1Cre/Kras G12D/Stat3C
e
Ptf1Cre/Kras G12D /TGFβR2 flox/flox
X
Stat3 flox/flox
Ptf1Cre/Kras G12D/TGFβR2 KO/Stat3 KO
b
b'
KC
KC/Stat3C
p-Stat3 DAPI
p-397FAK/ DAPI
p-MLC2 DAPI
Picrosirius Red
CD68 DAPI
H&E
Nuclear p-Stat3 (%)
p-397FAK Positive (%)
p-MLC2 Positive (%)
Area Threshold (AU)
CD68 Positive (%)
f
f'
KTC KO
Control
Stat3 KO
p-Stat3 DAPI
p-397FAK DAPI
p-MLC2 DAPI
Picrosirius Red
Tenascin DAPI
CD68 DAPI
YAP DAPI
H&E
Nuclear p-Stat3 (%)
p-397FAK-Positive (%)
p-MLC2 Positive (%)
Area Threshold (AU)
TNC Positive (%)
CD68 Positive (%)
Nuclear YAP (%)
c
KC/Stat3C (n=12)
KC (n=20)
p <0.0001
Percent Survival (%)
Time (days)
d
Elastic Modulus (Pa)
KC
KC/Stat3
g
KTC KO (n=19)
KTC KO/Stat3 KO(n=47)
p<0.001
Percent survival
Time (days)
h
Elastic Modulus (Pa)
KTC
KTC/ Stat3KO

figure 5

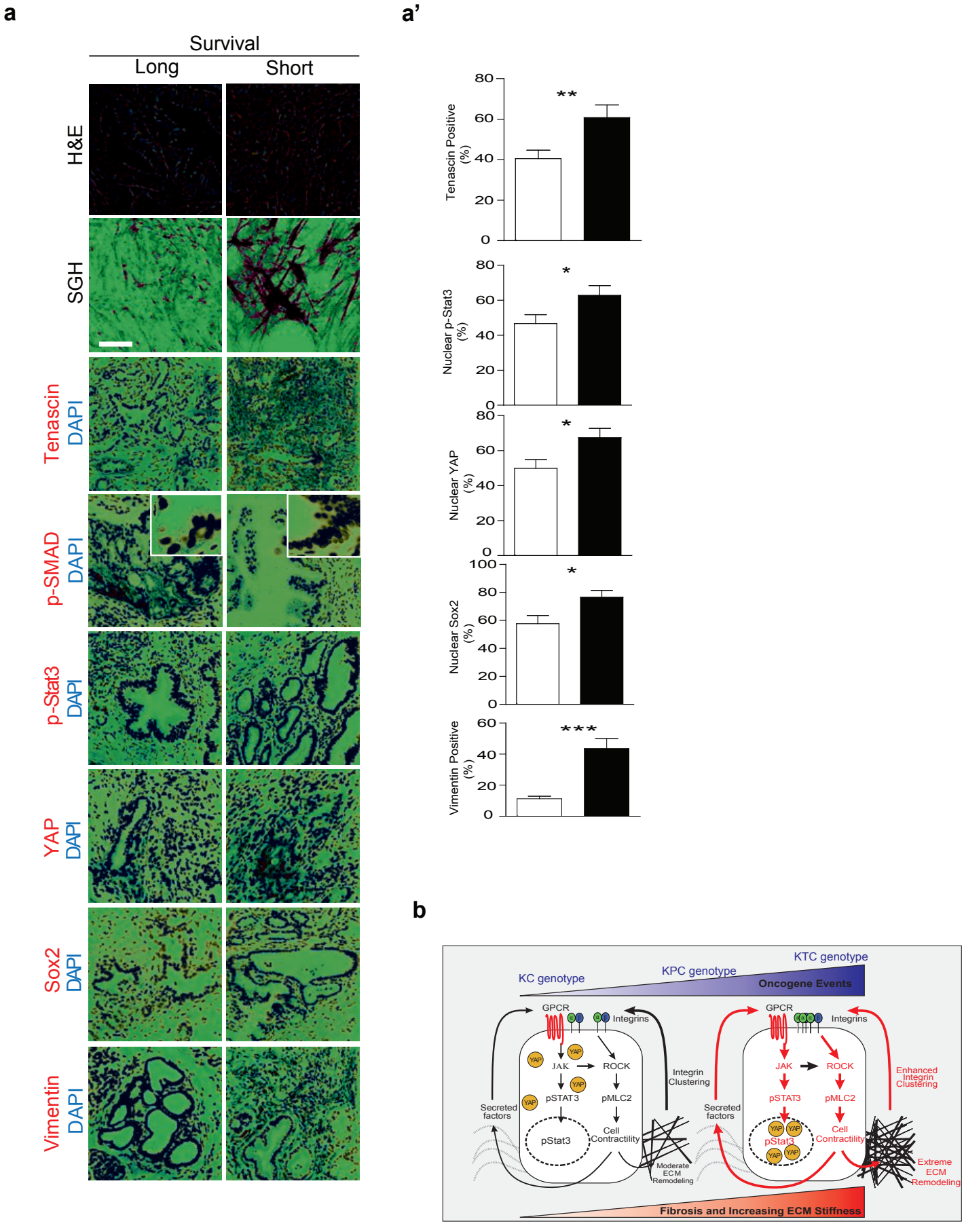

figure 6

□ Long Survival ■ Short Survival

Supplemental experimental procedures

Cell culture and establishment of primary pancreatic cell lines

Establishment of primary pancreatic tumor cells was performed as described previously (Aguirre et al., 2003). Cells were maintained in RPMI-1640 medium containing 10% FBS (Clontech). All experiments were performed within eight passages to avoid possible gross genomic changes during long-term in vitro culture. Derivative cells were transduced in vitro with a lentiviral vector-encoding firefly Luciferase and mApple fluorescent protein for combined bioluminescent imaging and flow sorting. To ensure that all cell lines expressed similar levels of luciferase, mApple expressing cells were flow sorted prior to injection into animals.

Lentiviral shRNA constructs

The clone IDs for shRNA are as follows: sh-ROCK1(TRCN0000022903), sh-FAK (TRCN0000023485) and eEGFP as a non specific control cloned into the lentiviral pLKO.1 puro vector (Sigma-Aldrich).

Preparation of luciferase-mApple Virus-Infected Cells

Lentivirus infection was performed with pLKO EEF1α mApple luc2 lentiviral vector for combined flow sorting and *in vivo* imaging. This was constructed from the pLKO.1 puro vector by inserting an in-frame fusion of mApple with the human codon optimized firefly luciferase gene from pGL4.10[luc2] (Promega) and placing this under control of the human EEF1α promoter. This cassette, followed by a WPRE element was inserted in place of the U6 cppt mPGK puro elements in pLKO.1 puro (from claI to kpnI sites).

Quantitative real-time PCR

RNA was extracted using trizol/chloroform isolation followed by Ambion mirVana kit (AM1560). Total RNA was reverse-transcribed using random primers (Amersham Biosciences), and β-actin primers were used to control for cDNA concentration in a separate PCR reactions for each sample. LightCycler Fast Start DNA Master SYBR Green Mix (Roche) was added to each PCR reaction along with cDNA and 1 pmol primer in a total volume of 10 µl. qPCR was performed on a eppendorf realplex2 mastercycler using the real-time primers provided,

according to instructions. Ct values were converted to fold expression changes ($2^{-\Delta\Delta Ct}$ values) following normalization to β-actin.

Primer sequences are listed below.

Gene	Sequence
CTGF	F 5'-GTGAGTCCTTCCAAAGCAGC-3' R 5'-TAGTTGGGTCTGGGCCAAAT-3'
β-actin	F 5'-GTGGGCCGCCCTAGGCACCA-3' R 5'-CGGTTGGCCTTAGGGTTCAGGG-3'

Flow sorting

Weighed tumors were minced and allowed to digest in a mixture of 1mg/ml of collagenase P (Roche 11213857001), 0.1 mg/ml Collagenase I (Sigma, C0130), 0.1 mg/ml Dispase II (Roche, 04942078001) and DNase (5MU/ml, Calbiochem, 260913) in DMEM media at 37°C for 30 min. The tissue lysate was filtered through a 40 μm mesh prior to immunostaining. The resulting single-cell suspension was stained with fixable viability dye eFluor 780, anti-CD45-APC-Cy7 (103115), anti-CD11b-FITC (101205) and anti-Ly6/C-PE (128007) (all from BioLegend). The percentage of positive cells were analyzed by FlowJo and gated on CD45 positivity. Unstained, live/dead only, and single stain served as control. Doublets were gated out using forward-scatter width/height and sidewardscatter width/height event characteristics.

Antibodies and reagents

Antibodies were as follows: a-SMA (Sigma-Aldrich C6198), GLi-1 (Thermo Scientific PA5-32206), LOX (Imgenex IMG-6442A), YAP (Cell signaling 4912) β1integrin (EMD Millipore MABT409), pY397-FAK (Invitrogen 44625), total FAK (BD Biosciences 610088), ROCK (Cell Signaling C8F7), p-MLC2 (Cell Signaling 3671), p-MyPT1 (Millipore ABS45), p-Stat3 (Cell Signaling 9145), total Stat3 (Cell Signaling 9132), GAPDH (Cell Signaling 2118), CD45 (BD Biosciences 550539), CD68 (Thermo Scientific Ab-3), Alexa Fluor-conjugated goat secondary anti–mouse IgG and anti–rabbit IgG antibodies (Invitrogen A11012 and A11005) and HRP-conjugated rabbit secondary antibody (GE health care life sciences NA934VS).

Supplementary Figure Legends

Figure S1.

(a) Representative second harmonic generation (SHG) images of extracellular collagen architecture and distribution in the pancreatic tissue from 8 week old pancreatic tissue excised from mice expressing Kras (KC), Kras with one mutant allele of P53 (KPC) or Kras with heterozygous loss of the Tgfbr2 receptor in the pancreatic epithelium (KTC) (1st panel). Scale bar, 75µm. Representative force maps measured using atomic force microscopy (AFM) indentation of the stiffness of the extracellular matrix surrounding the pancreatic ductal lesions developing in the 8 week old animals (1st panel insert). Representative immunofluorescence images of pancreatic tissue described above stained for pMLC2 (red, 2nd panel), ß1integrin/^{p397}FAK (green/red, 3rd panel), pMyPT1 (red, 4th panel), YAP (red, 5th panel) and DAPI (blue). Scale bar, 50µm. **(a').** Bar graphs quantifying the fibril thickness and distribution imaged by SHG around the developing pancreatic ductal lesions of pancreatic tissue described above. **(a")** Bar graphs showing the distribution of the stiffness of the extracellular matrix surrounding the normal and developing lesions in tissue described above as measured by AFM indentation. **(b)** Bar graphs quantifying the tissue images shown in the panels in a and in Fig. 1a.

Figure S2.

(a) Representative immunofluorescence images of pancreatic tissues stained for Collagen 3 (green, 1st panel), FAP (green, 2nd panel), Gli1 (green, 3rd panel), αSMA (green, 4th panel) and DAPI (blue) from 20 weeks old tissue excised from mice expressing Kras with one mutant allele of P53 (KPC) and Kras with heterozygous loss of the Tgfbr2 in the pancreatic epithelium (KTC). Scale bar, 75 µm. **(b)** Representative immunofluorescence images of pancreatic tissues stained for ß1integrin/^{p397}FAK (green/red, top panel), YAP (red, bottom panel) and DAPI (blue) from 20 weeks old tissue excised from mice expressing Kras with heterozygous loss of the P53 (KP-Ptf1a-C) and Kras with heterozygous loss of the Tgfbr2 in the pancreatic epithelium (KTC). Scale bar, 50 µm. For *in vivo* experiments, N=5 mice per group. *p<0.05; **p<0.01, ***p<0.001, ****p<0.0001, "ns" denotes not significant).

Figure S3.

(a) Representative images of collagen gels incubated with KC, KPC or KTC pancreatic epithelial tumor cells or with KTC cells treated with vehicle or the ROCK inhibitor Y27632. **(a')** Bar graphs quantifying the mean collagen fiber diameter in the three-dimensional collagen gels

described in a. **(b)** Representative immunoblot showing ROCK protein levels in KTC tumor cells expressing either a control shRNA or an shRNA to ROCK. Results are normalized to GAPDH. **(b')** Bar graph showing the quantification of b. **(c)** Representative bioluminescence images of tumor growth in nude mice 3 weeks after injection with KC, KPC, KTC and KTC pancreatic tumor cells expressing either a control shRNA or an shRNA to ROCK. **(c')** Bar graph showing the weight of the pancreatic tumors generated by the KC, KPC and KTC pancreatic epithelial cancer cells. **(c")** and **(c"')** Bar graphs quantifying CTGF mRNA expression for pancreatic tumors described in c. Results are normalized to β-actin. For *in vitro* bar graphs, results are the mean +/- SEM of at least 3 independent experiments. For *in vivo* experiments, N=5 mice per group. (*p<0.05; **p<0.01, ***p<0.001, ****p<0.0001, "ns" denotes not significant).

Figure S4.

(a) Representative immunofluorescence images of pancreatic tissue excised from 8 week old KC, KPC and KTC mice stained for pStat3 (red) and DAPI (blue). Scale bar, 50μm. **(a')** Bar graphs quantifying the level of stromal versus epithelial pStat3 in the tissues stained in a. **(b)** Representative images of three-dimensional collagen gels incubated with KTC pancreatic epithelial tumor cells for 24 hours either with vehicle or the JAK inhibitor Ruxolitinib. **(c)** Representative images of three-dimensional collagen gels incubated with KC tumor cells treated with vehicle or the conditioned media from 48 hour cultured KTC tumor cells. **(d)** Representative immunoblot showing total (Stat3) and activated Stat3 (pStat3) levels in KTC tumor cells cultured on soft or stiff polyacrylamide substrates. **(d')** Bar graph showing the quantification of d. **(e)** Representative cytokines array images measured in the conditioned media of KC and KTC cells cultured on soft or soft polyacrylamide substrates. For *in vitro* bar graphs, results are the mean +/- SEM of at least 3 independent experiments. For *in vivo* experiments, N=5 mice per group. (*p<0.05; **p<0.01, ***p<0.001, ****p<0.0001, "ns" denotes not significant).

Figure S5.

(a) Graphic of mouse manipulations used to study the impact of β1V737N expression in the pancreatic epithelium on tissue fibrosis. **(b)** Representative immunofluorescence images of pancreatic tissues excised from 3 month old control and β1V737N mice stained for ^{p397}FAK (top panel; red) and pMLC2 (2nd panel; red), pStat3 (5th panel; red), scale bar, 50 μm, CD45 (6th panel; red) and CD68 (7th panel; red), scale bar, 100μm, and DAPI (blue). **(b)** (3rd panel)

Representative polarized light images of collagen fibers revealed by picrosirius red (PR) staining of pancreatic tissue described above. Scale bar, 75μm. **(b)** (4^{th} panel) Representative force maps of ECM stiffness measured using AFM indentation in pancreatic tissue described above. **(b')** Bar graphs quantifying the tissue images shown in the panels in b. **(c)** Bar graphs quantifying CTGF mRNA expression for pancreatic tissue shown in b. Results are normalized to β-actin. **(d)** Bar graphs showing quantification of total pancreatic CD45+ and Ly6C immune cells as determined by flow cytometry. **(e)**. Representative cytokines array images measured in pancreatic tissue shown in b. **(e')** Bar graphs showing quantification of cytokine levels shown in e.

Figure S6.

(a) Representative immunofluorescence images of 6 week old pancreatic tissue excised from β1V737N mice treated with vehicle or the FAK inhibitor PND-1186 stained for ^{p397}FAK (top panel; red), pMLC2 (2^{nd} panel; red), pStat3 (5^{th} panel; red), scale bar, 50 μm, CD45 (6^{th} panel), CD68 (7^{th} panel; red) and DAPI (blue). Scale bar, 100μm. **(a)** (3^{rd} panel) Representative polarized light images of collagen fibers revealed by PR staining of pancreatic tissue described above. Scale bar, 75μm. **(a)** (4^{th} panel) Representative maps of ECM stiffness measured using AFM indentation in pancreatic tissue described above. **(a')** Bar graphs quantifying the tissue images shown in the panels in a.

Figure S7.

(a) Representative immunoblot showing FAK level in KTC tumor cells expressing either a control shRNA or an shRNA to FAK. Results are normalized to GAPDH. **(a')**. Bar graph showing the quantification of a. **(b)** Representative bioluminescence images of tumor growth in nude mice 3 weeks after injection with KTC pancreatic tumor cells expressing either a control shRNA or an shRNA to FAK. **(c)** Bar graphs showing quantification of total pancreatic Ly6C and CD11b immune cells as determined by flow cytometry. **(d)** Representative cytokines array images measured in KC and KC/β1V737N pancreatic tissue. **(d')**. Bar graph showing the quantification of d.

Figure S8.

(a) Representative immunofluorescence images of pancreatic tissues excised from 5 week old control, KC and homozygous KTC (KTC KO) mice stained for LOX (top panel; red), scale bar 50 μm, YAP (3^{rd} panel, red), ^{p397}FAK (4^{th} panel, red) and p-MLC2 (5^{th} anel, red) and pStat3 (6^{th} panel, red) scale bar 20 μm, and DAPI (blue). **(a)** (2^{nd} panel) Representative polarized light

images of collagen fibers revealed by PR staining of pancreatic tissue described above. Scale bar, 75µm. a'. Bar graphs quantifying the tissue images shown in the panels in a. **(b)** Quantification of ECM stiffness measured by AFM in pancreatic tissue shown in a. For *in vivo* experiments, N=5 mice per group. (*p<0.05; **p<0.01, ***p<0.001, ****p<0.0001, "ns" denotes not significant).

Figure S9.

(a) Representative immunofluorescence images of pancreatic tissues excised from 5 week old control and Stat3C mice stained for pStat3 (top panel; red), scale bar, 75 µm, ^{p397}FAK (2nd panel; red) and pMLC2 (3rd panel; red), Scale bar, 50 µm, CD45 (5th panel; red), CD68 (6th panel; red), and DAPI (blue). Scale bar, 100µm. **(a)**. (4th panel) Representative polarized light images of collagen fibers revealed by PR staining of pancreatic tissue described above. Scale bar, 75µm. **(a)** (7th panel) Representative phase contrast images of H&E stained pancreatic tissue as described above. Scale bar, 100µm. **(a')** Bar graphs quantifying the tissue images shown in the panels in a. **(b)** Bar graphs quantifying CTGF mRNA expression for pancreatic tissue excised from 5 week old homozygous KTC (KTC KO) (Control) and KTC/Stat3 KO mice (Stat3 KO). Results are normalized to β-actin. **(c)** Immunofluorescence confocal images of pancreatic tissues from 6 week old KTC (het) mice treated with either vehicle or the JAK inhibitor Ruxolitinib stained for pStat3 (top panel; red), scale bar, 75 µm, ^{p397}FAK (2nd panel; red) and pMLC2 (3rd d panel; red), scale bar, 50 µm, CD45 (5th panel; red), CD68 (6th panel; red), scale bar, 100 µm, and DAPI (blue). **(c)** (4th panel) Representative polarized light images of collagen fibers revealed by PR staining of pancreatic tissue described above. Scale bar, 75µm. **(c)** (7th panel) Representative phase contrast images of H&E stained pancreatic tissue as described above. Scale bar, 100µm. **(c')**. Bar graphs quantifying the tissue images shown in the panels in c. **(d)** Quantification of ECM stiffness measured by AFM in pancreatic tissue shown in c. **(e)** bar graphs quantifying the weight of the pancreatic tumors shown in c. For *in vivo* experiments, N=5 mice per group. (*p<0.05; **p<0.01, ***p<0.001, ****p<0.0001, "ns" denotes not significant).

Individual Genes Used for Survival Analysis of GSE21501
COL1A2
COL2A1
COL3A1
COL4A1
COL5A1
COL11A1
COL24A1
COL27A1

Protein	Functional	Matrisome	MW	GENE	nmol protein/gram of tissue											KPC/KC	p value	KTC/KC	p value	KTC/KPC	p value	Analytical CV(%)
					KC1	KC2	KC3	Avg.	KPC1	KPC2	KPC3	Avg.	KTC1	KTC2	KTC3	Avg.							
Collagen alpha-1/5(IV) chain(Arresten/Core Protein)	Basement Membrane	Collagen	160613	COL4A1*	0.394	0.345	0.444	0.394	0.385	0.376	0.506	0.422	0.315	0.405	0.406	0.375	1.071	0.611	0.952	0.674	0.889	0.415	16%
Collagen alpha-1/5(IV) chain(Arresten/Core Protein)	Basement Membrane	Collagen	160613	COL4A1/5*	0.398	0.300	0.472	0.390	0.404	0.485	0.458	0.449	0.380	0.427	0.466	0.424	1.151	0.345	1.087	0.574	0.944	0.508	22%
Collagen alpha-2(IV) chain	Basement Membrane	Collagen	161386	COL4A2	0.210	0.153	0.236	0.200	0.202	0.228	0.198	0.209	0.188	0.238	0.213	0.213	1.047	0.735	1.065	0.669	1.017	0.844	14%
Collagen alpha-2(IV) chain(Canstatin/Core Protein)	Basement Membrane	Collagen	161386	COL4A2*	0.183	0.142	0.159	0.161	0.135	0.135	0.199	0.156	0.141	0.186	0.171	0.166	0.968	0.845	1.027	0.819	1.060	0.727	12%
Collagen alpha-1(XIV) chain	FACIT Collagen	Collagen	191772	COL14A1	0.930	1.374	1.525	1.276	1.729	1.174	1.567	1.490	0.788	0.767	1.043	0.866	1.168	0.428	0.678	0.108	0.581	0.029	14%
Collagen alpha-1(I) chain	Fibrillar Collagen	Collagen	137953	COL1A1	34.029	32.264	39.162	35.151	30.428	31.711	33.976	32.038	24.743	36.783	35.071	32.199	0.911	0.250	0.916	0.529	1.005	0.969	10%
Collagen alpha-1(I) chain(C-term Propeptides (NC1 Domain))	Fibrillar Collagen	Collagen	137953	COL1A1*	0.105	0.092	0.088	0.095	0.099	0.097	0.088	0.095	0.154	0.139	0.095	0.129	1.002	0.979	1.365	0.133	1.363	0.128	12%
Collagen alpha-1(I) chain(fragment)	Fibrillar Collagen	Collagen	137953	COL1A1*	11.932	7.104	9.720	9.585	5.635	7.261	10.343	7.747	7.102	8.617	8.663	8.127	0.808	0.402	0.848	0.382	1.049	0.809	20%
Collagen alpha-2(I) chain	Fibrillar Collagen	Collagen	129564	COL1A2	21.979	20.899	25.083	22.653	19.124	21.568	22.606	21.099	18.913	28.415	23.075	23.468	0.931	0.393	1.036	0.801	1.112	0.465	14%
Collagen alpha-1(V) chain	Fibrillar Collagen	Collagen	183987	COL5A1	0.847	1.200	1.219	1.089	1.252	1.170	1.344	1.255	0.789	0.763	0.868	0.807	1.153	0.273	0.741	0.087	0.643	0.002	25%
Collagen alpha-2(V) chain	Fibrillar Collagen	Collagen	145018	COL5A2	0.545	0.423	0.733	0.567	0.564	0.590	0.541	0.565	0.314	0.551	0.426	0.430	0.997	0.987	0.759	0.295	0.762	0.125	11%
Collagen alpha-1(XVII) chain	Matricellular	Collagen	143568	COL17A1	0.069	0.140	0.152	0.120	0.113	0.130	0.120	0.121	0.252	0.133	0.191	0.192	1.009	0.968	1.594	0.173	1.580	0.114	26%
Collagen alpha-1(XVIII) chain	Matricellular	Collagen	182881	COL18A1	0.029	0.018	0.030	0.026	0.038	0.013	0.033	0.028	0.015	0.027	0.013	0.018	1.084	0.809	0.703	0.255	0.649	0.321	12%
Collagen alpha-1(VI) chain	Matricellular	Collagen	108806	COL6A1	2.442	2.497	3.841	2.927	3.242	1.831	3.532	2.869	1.298	2.233	1.508	1.680	0.980	0.938	0.574	0.081	0.586	0.117	15%
Collagen alpha-2(VI) chain	Matricellular	Collagen	108579	COL6A2	3.466	3.546	4.209	3.740	4.491	3.226	4.890	4.202	1.611	2.959	2.431	2.334	1.124	0.451	0.624	0.037	0.555	0.043	14%
Collagen alpha-3(VI) chain	Matricellular	Collagen	288133	COL6A3	1.414	1.440	1.504	1.453	1.495	0.391	1.296	1.061	0.327	0.652	0.724	0.568	0.730	0.314	0.391	0.002	0.535	0.244	16%
Collagen alpha-1(VII) chain(Fibronectin type-III 3 Domain)	Matricellular	Collagen	295092	COL7A1*	0.008	0.012	0.014	0.011	0.009	0.008	0.015	0.011	0.011	0.037	0.014	0.021	0.955	0.866	1.887	0.307	1.975	0.291	14%
Collagen alpha-1(VII) chain(Fibronectin type-III 1 Domain)	Matricellular	Collagen	295092	COL7A1*		0.013	0.012	0.012	0.012	0.013	0.012	0.013	0.015	0.032		0.024	1.001	0.972	1.882	0.318	1.879	0.176	25%

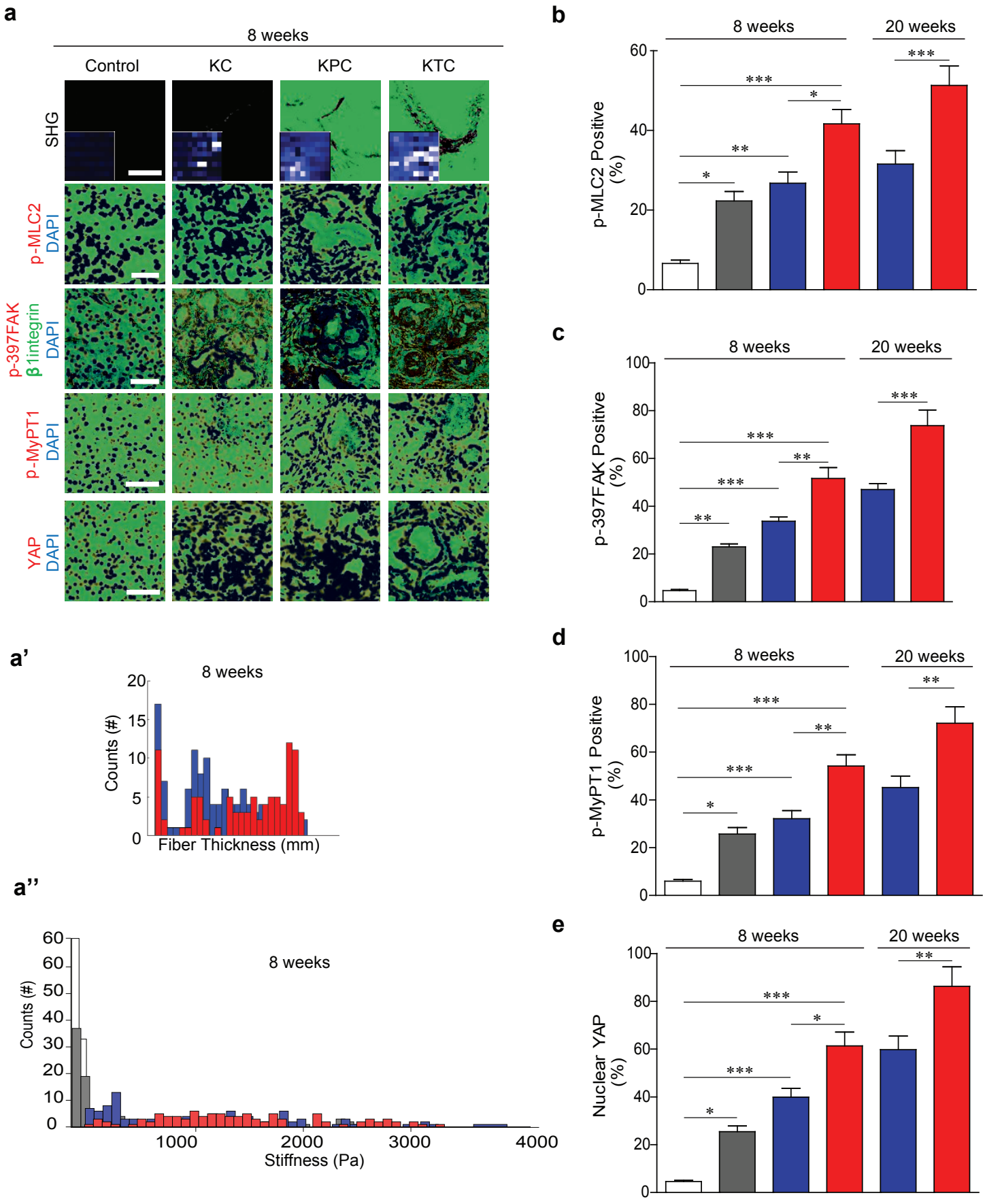
a
8 weeks
Control
KC
KPC
KTC
SHG
p-MLC2
DAPI
p-397FAK
β1integrin
DAPI
p-MyPT1
DAPI
YAP
DAPI
a'
8 weeks
Counts (#)
Fiber Thickness (mm)
a''
8 weeks
Counts (#)
Stiffness (Pa)
b
8 weeks
20 weeks
p-MLC2 Positive (%)
c
8 weeks
20 weeks
p-397FAK Positive (%)
d
8 weeks
20 weeks
p-MyPT1 Positive (%)
e
8 weeks
20 weeks
Nuclear YAP (%)

Figure S1

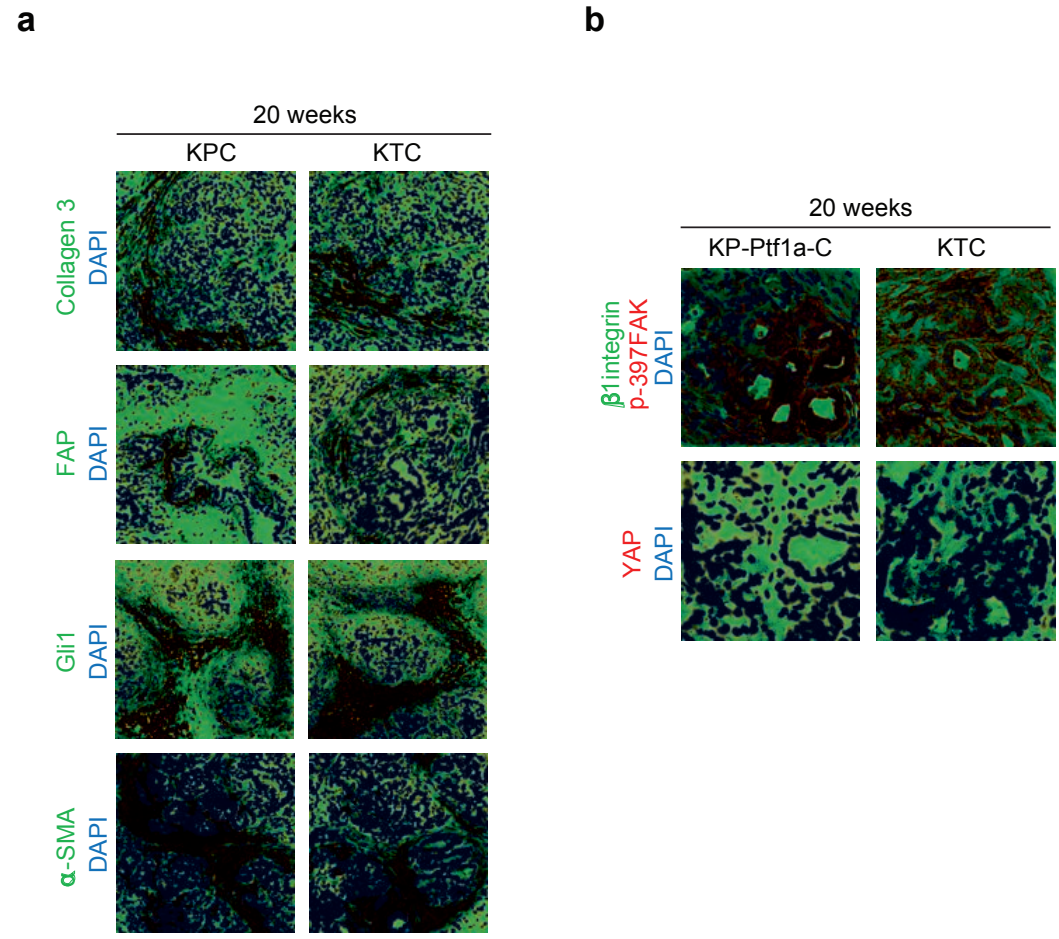
a
20 weeks
KPC
KTC
Collagen 3
DAPI
FAP
DAPI
Gli1
DAPI
α-SMA
DAPI
b
20 weeks
KP-Ptf1a-C
KTC
β1integrin
p-397FAK
DAPI
YAP
DAPI

Figure S2

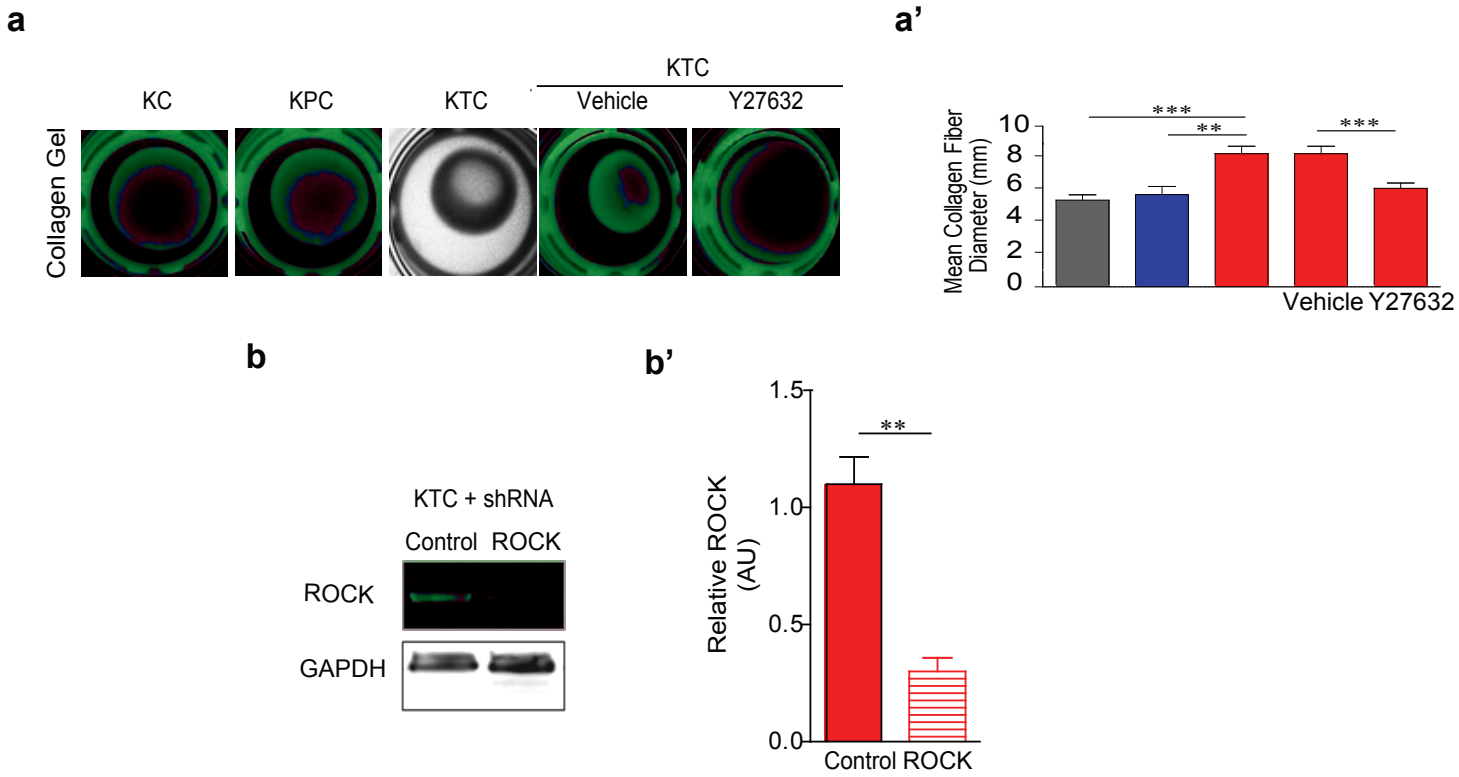
a
KC
KPC
KTC
KTC
Vehicle
Y27632
Collagen Gel
a'
Mean Collagen Fiber Diameter (mm)
***
**
***
Vehicle Y27632
b
KTC + shRNA
Control ROCK
ROCK
GAPDH
b'
Relative ROCK (AU)
**
Control ROCK
c
KC
KPC
KTC
KTC + shRNA
Control
ROCK
Luminescence
15K
10K
5K
c'
Tumor Weight (grams)
***
***
***
Control ROCK
c''
CTGF mRNA (%)
***
c'''
CTGF mRNA (%)
*
Control ROCK
Control
KC
KPC
KTC

Figure S3

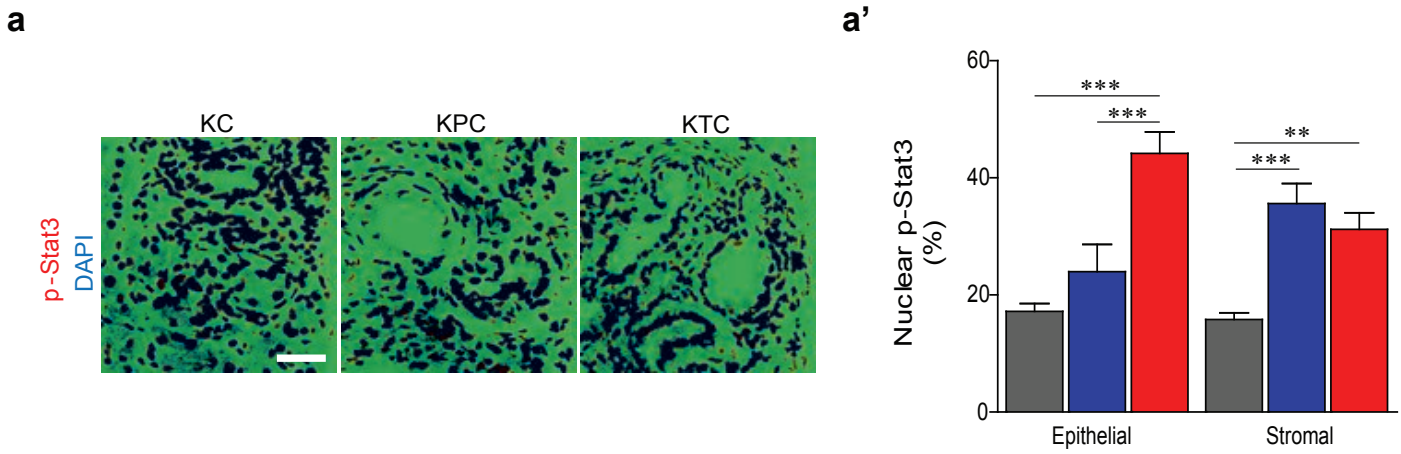

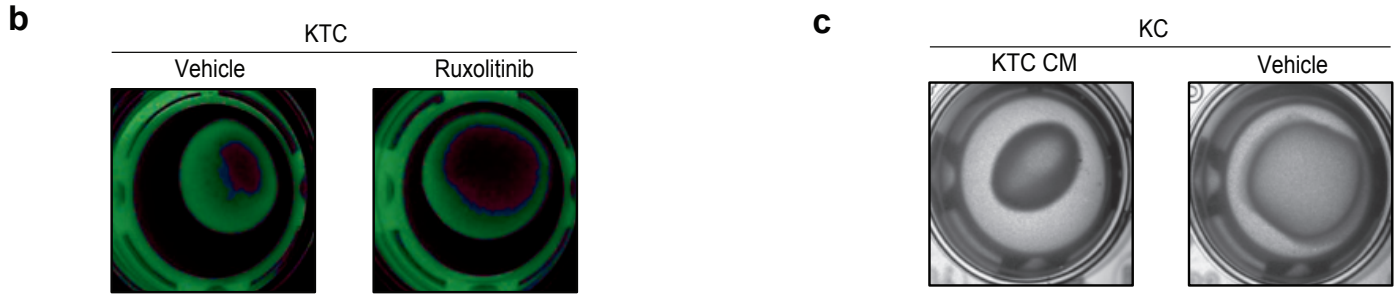

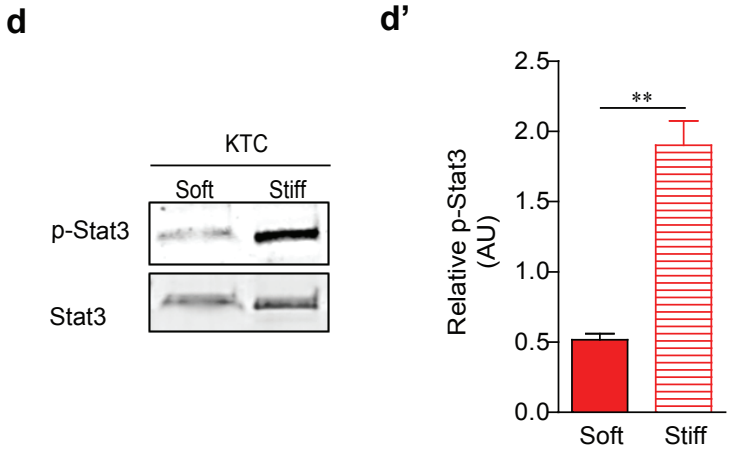

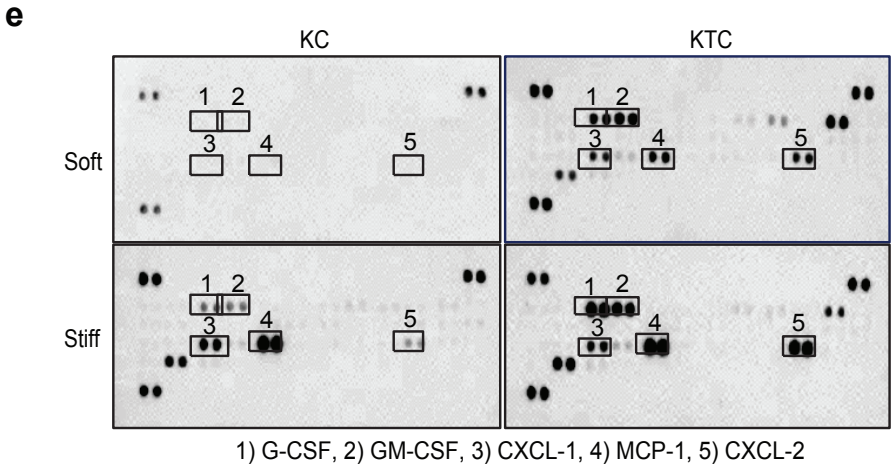

1) G-CSF, 2) GM-CSF, 3) CXCL-1, 4) MCP-1, 5) CXCL-2

Control KC KPC KTC

Figure S4

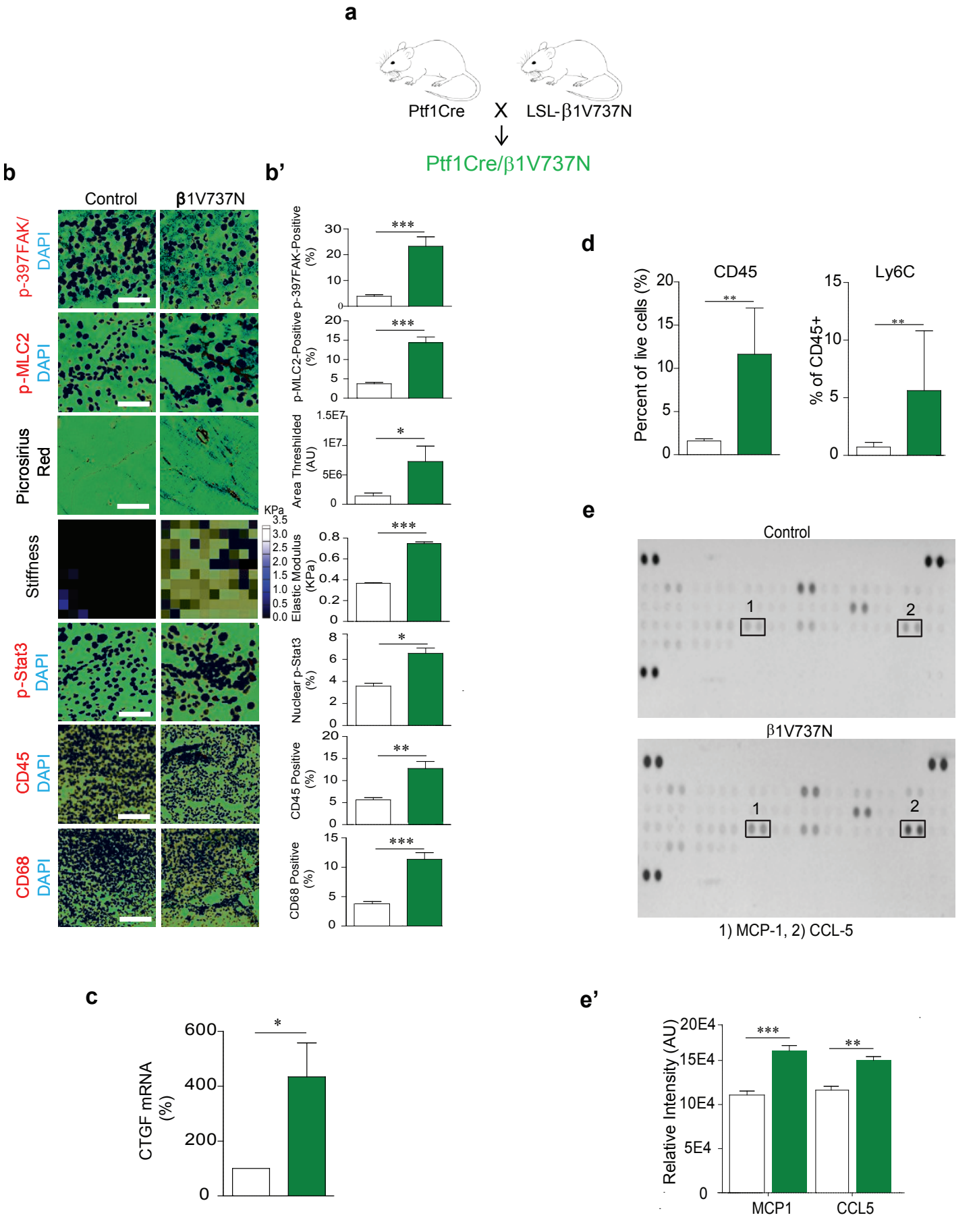
a
Ptf1Cre
X
LSL-β1V737N
Ptf1Cre/β1V737N
b
Control
β1V737N
p-397FAK/ DAPI
p-MLC2 DAPI
Picrosirius Red
Stiffness
p-Stat3 DAPI
CD45 DAPI
CD68 DAPI
KPa
3.5
3.0
2.5
2.0
1.5
1.0
0.5
0.0
b'
p-397FAK-Positive (%)
p-MLC2-Positive (%)
Area Thresholded (AU)
Elastic Modulus (KPa)
Nuclear p-Stat3 (%)
CD45 Positive (%)
CD68 Positive (%)
d
CD45
Ly6C
Percent of live cells (%)
% of CD45+
e
Control
β1V737N
1
2
1) MCP-1, 2) CCL-5
c
CTGF mRNA (%)
e'
Relative Intensity (AU)
MCP1
CCL5
Control
β1V737N

Figure S5

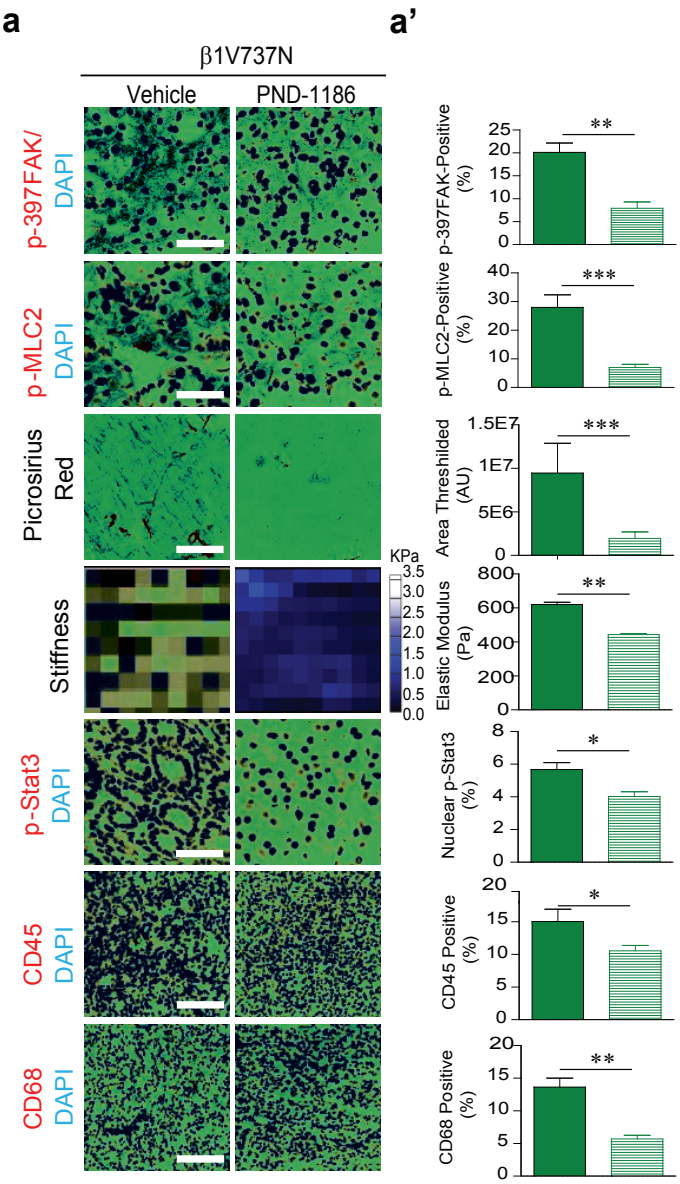
a
a'
β1V737N
Vehicle
PND-1186
p-397FAK/ DAPI
p-MLC2 DAPI
Picrosirius Red
Stiffness
p-Stat3 DAPI
CD45 DAPI
CD68 DAPI
KPa
3.5
3.0
2.5
2.0
1.5
1.0
0.5
0.0
p-397FAK-Positive (%)
p-MLC2-Positive (%)
Area Threshilded (AU)
Elastic Modulus (Pa)
Nuclear p-Stat3 (%)
CD45 Positive (%)
CD68 Positive (%)
Vehicle
PND-1186

Figure S6

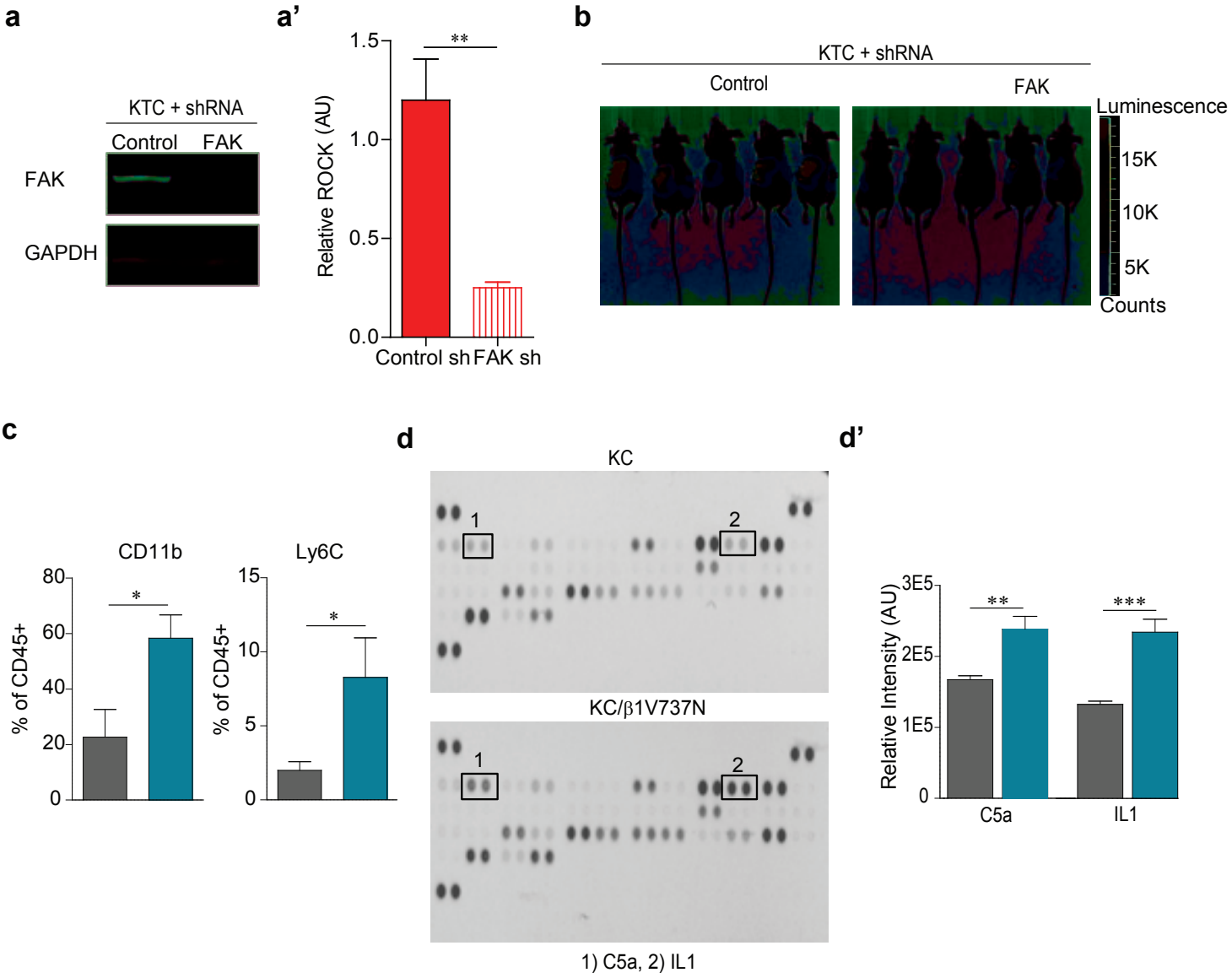
a
KTC + shRNA
Control
FAK
FAK
GAPDH
a'
Relative ROCK (AU)
1.5
1.0
0.5
0.0
**
Control sh
FAK sh
b
KTC + shRNA
Control
FAK
Luminescence
15K
10K
5K
Counts
c
CD11b
% of CD45+
80
60
40
20
0
*
Ly6C
% of CD45+
15
10
5
0
*
d
KC
1
2
KC/β1V737N
1
2
1) C5a, 2) IL1
d'
Relative Intensity (AU)
3E5
2E5
1E5
0
**
***
C5a
IL1
KTC
KC
KC/β1V737N

Figure S7

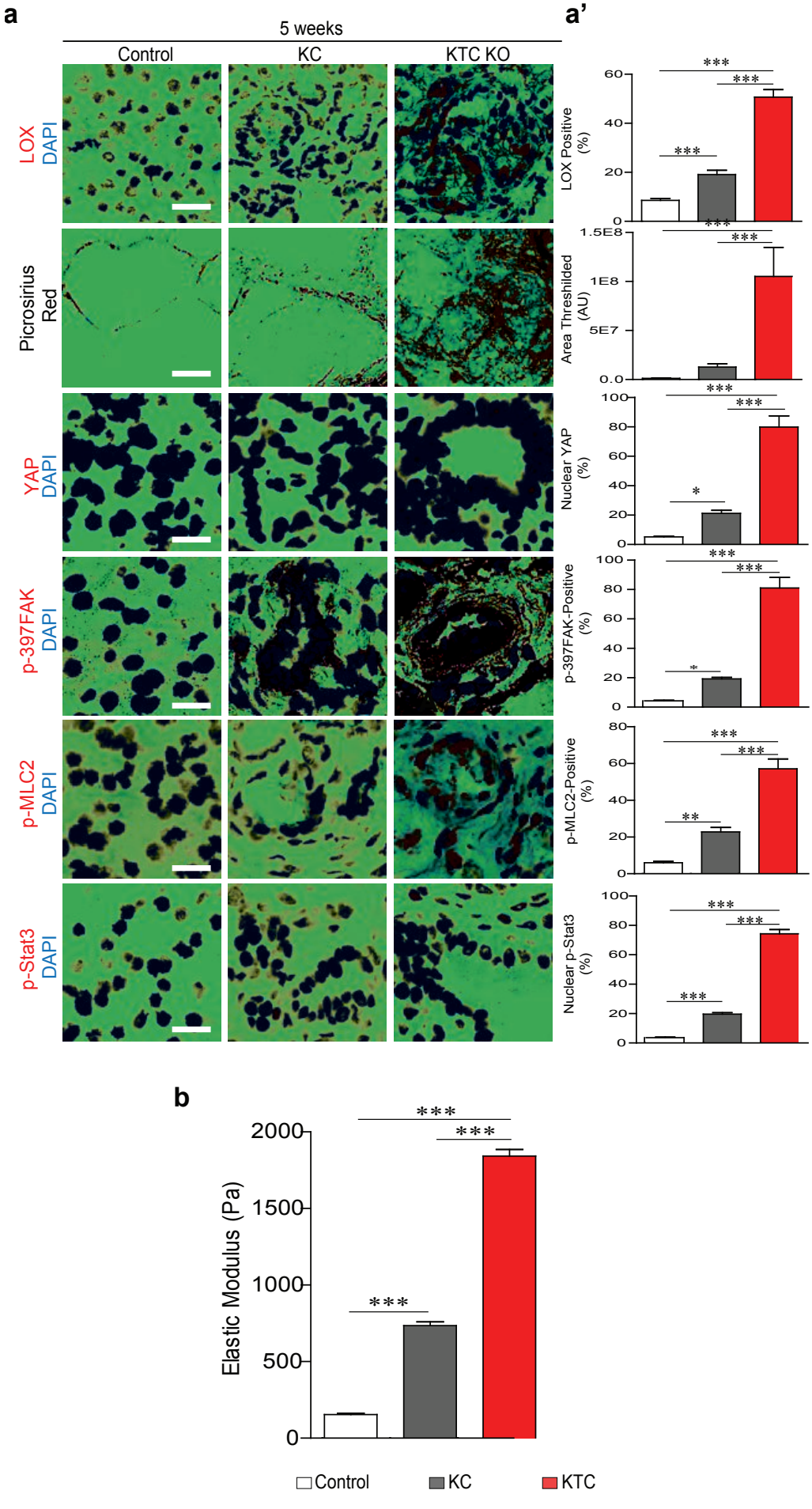
a
5 weeks
Control
KC
KTC KO
LOX
DAPI
Picrosirius
Red
YAP
DAPI
p-397FAK
DAPI
p-MLC2
DAPI
p-Stat3
DAPI
a'
LOX Positive (%)
Area Thresholded (AU)
Nuclear YAP (%)
p-397FAK-Positive (%)
p-MLC2-Positive (%)
Nuclear p-Stat3 (%)
b
Elastic Modulus (Pa)
Control
KC
KTC

Figure S8

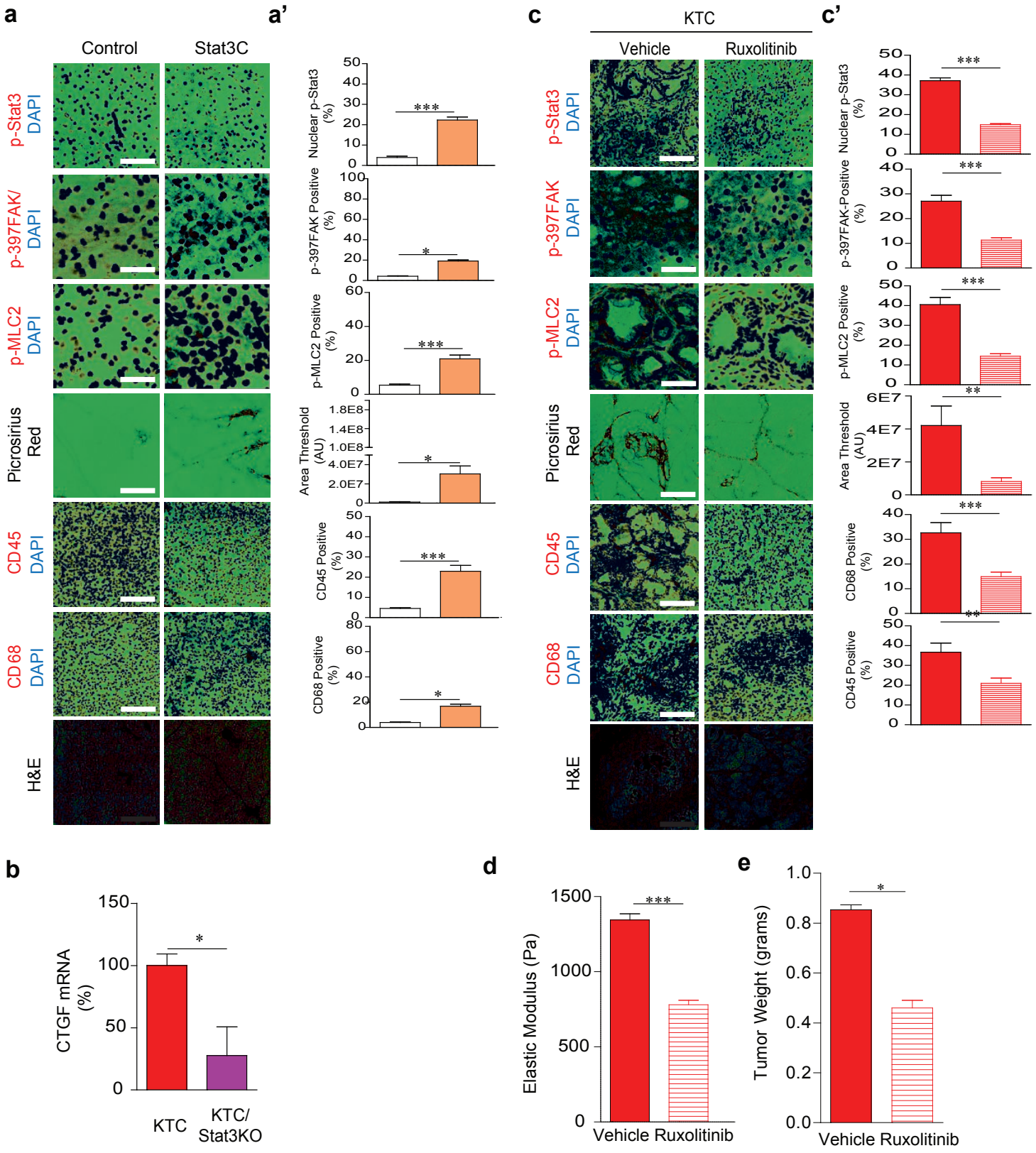
a
a'
c
c'
Control
Stat3C
KTC
Vehicle
Ruxolitinib
p-Stat3 DAPI
p-397FAK/ DAPI
p-MLC2 DAPI
Picrosirius Red
CD45 DAPI
CD68 DAPI
H&E
Nuclear p-Stat3 (%)
p-397FAK Positive (%)
p-MLC2 Positive (%)
Area Threshold (AU)
CD45 Positive (%)
CD68 Positive (%)
b
CTGF mRNA (%)
KTC
KTC/ Stat3KO
d
Elastic Modulus (Pa)
Vehicle Ruxolitinib
e
Tumor Weight (grams)
Vehicle Ruxolitinib

Figure S9